Cationic π-Conjugated Polyelectrolyte Shows Antimicrobial Activity by Causing Lipid Loss and Lowering Elastic Modulus of Bacteria

Ehsan Zamani,[1,†] Tyler J. Johnson,[1,†] Shyambo Chatterjee,[1] Cheryl Immethun,[1] Anandakumar Sarella,[2] Rajib Saha,[1] Shudipto Konika Dishari[1,*]

[1,] Department of Chemical and Biomolecular Engineering, University of Nebraska-Lincoln, Lincoln, Nebraska 68588, United States*

[2] Nebraska Center for Materials and Nanoscience, Voelte-Keegan Nanoscience Research Center, University of Nebraska-Lincoln, Lincoln, NE 68588-0298, United States

[†] E.Z. and T.J.J. contributed equally to this work.

KEYWORDS: *Antimicrobial, cationic conjugated polyelectrolytes, antibiotic-resistant, outer membrane, elastic modulus, lipid loss.*

ABSTRACT: Cationic, π-conjugated oligo-/polyelectrolytes (CCOEs/CCPEs) have shown great potential as antimicrobial materials to fight against antibiotic resistance. In this work, we treated wild-type and ampicillin-resistant (amp-resistant) *Escherichia coli (E. coli)* with a promising cationic, π-conjugated polyelectrolyte (P1) with phenylene-based backbone and investigated the resulting morphological, mechanical, and compositional changes of the outer membrane of bacteria in great detail. The cationic quaternary amine groups of P1 led to electrostatic interactions with negatively-charged moieties within the outer membrane of bacteria. Using atomic force microscopy (AFM), high-resolution transmission electron microscopy (TEM), we showed that due to this treatment, the bacterial outer membrane became rougher, decreased in stiffness/elastic modulus (AFM nanoindentation), formed blebs, and released vesicles near the cells. These evidences, in addition to increased staining of P1-treated cell membrane by lipophilic dye Nile Red (confocal laser scanning microscopy (CLSM)), suggested loosening/disruption of packing of the outer cell envelope and release and exposure of lipid-based components. Lipidomics and fatty acid analysis confirmed a significant loss of phosphate-based outer membrane lipids and fatty acids some of which are critically needed to maintain cell wall integrity and mechanical strength. Lipidomics and UV-Vis analysis also confirmed that the extracellular vesicles released upon treatment (AFM) are composed of lipids and cationic P1. Such surface alterations (vesicle/bleb formation) and release of lipids/fatty acids upon treatment were effective enough to inhibit further growth of *E. coli* cells without completely disintegrating the cells and have been known as a defense mechanism of cells against cationic antimicrobial agents.

INTRODUCTION

Continuous evolution of bacteria and antibiotic resistance poses a severe threat to animals and humans.[1–3] Coates et al.[4] suggested that at least 20 new classes of antibiotics are required to be developed between 2000 and 2050 to fight against antimicrobial resistance, whereas only two new classes of antibiotics have been developed during the past two decades.[1,5] While the productivity of antibiotic research is impacted by many issues,[1,6] the successful development of novel and effective antibiotics greatly relies on our understanding of cell-drug interactions. The cell wall of a bacteria, as the first line of defense against antimicrobial agents,[7] gives mechanical integrity to the cell and is responsible for selectively transporting materials inside/outside of the cell.[8] Also, bacteria often show antibiotic resistance by altering their outer cell envelopes.[9–13] The outer cell envelope of a typical Gram-negative bacteria contains an outer membrane, and an inner membrane which are separated by a periplasmic space.[14] The outer membrane of Gram-negative bacteria can be divided into five regions: O-antigen (includes, glucosamine, galactosamine), outer core (includes, sugars such as D-glucose, D-mannose, D-galactose), inner core (includes, sugars such as heptose and keto-deoxyoctulosonate (KDO)), lipid A (includes, phosphorylated glucosamine disaccharide functionalized with fatty acids), and a phospholipid layer[15] forming a lipid bilayer with lipid A (glycerol-based backbone having hydrophilic, phosphate-containing head groups, and hydrophobic tails derived from fatty acids) (Figure S1)).[16,17,18–20,21,22] On the other hand, the inner membrane consists of a phospholipid-based bilayer.[23] The components of the outer cell envelope are crucial, especially the charged lipid-based components as they are often susceptible to attack by oppositely charged antimicrobial compounds, such as cationic antimicrobial peptides (AMPs),[24–30] and cationic π-conjugated oligo/polyelectrolytes (CCOEs/CCPEs).[26,31–39]

In the last few years, CCOEs/CCPEs have grabbed significant attention for their potential in killing or inhibiting the growth of both wild-type and antibiotic (such as β-lactams)-resistant bacteria (light assisted/dark mode).[26,31–38] They are very attractive because some of the cationic π-conjugated molecules showed effectiveness against bacteria, such as *Enterococcus faecalis* (*E. faecalis*) which can grow in harsh environments.[33] Moreover, such bacterial strains showing resistance to traditional membrane-targeting antibiotics (e.g. daptomycin), found it difficult to show resistance against charged π-conjugated molecules[33] mainly due to their non-specific

binding nature to bacteria. Most of the CCOEs/CCPEs have been found to be inactive against mammalian cell membrane while showing activity against bacterial membrane or artificial lipid membranes[40,26] due to the abundance of negatively charged lipid moieties in bacterial outer membrane reachable by CCOEs/CCPEs.[41] Leveraging CCOEs/CCPEs interesting optical, electronic, and pathogen inactivation capabilities, many have proposed their applications in photodynamic therapies for tumor/cancer treatments and more.[35,42] All of these highlights the novelty of this class of antimicrobial molecules and the need to further explore and understand the mechanism of action of CCOEs/CCPEs against antibiotic-resistant bacteria.

Correlating structural features with cell membrane perturbation has been identified as a crucial first step to design new antimicrobial materials. In efforts to design and synthesize cationic π-conjugated molecules, phenylenevinylene,[38,43] phenyleneethylene,[26,36,34] imidazolium,[37] thiophene,[35,44,45] and fluorene[32]-backbone based antibacterial agents have been commonly reported. Bazan et al.[43,35,18,46] studied phenylenevinylene-based cationic π-conjugated molecules against both Gram-negative (*E. coli*) and Gram-positive (*E. faecalis*) bacteria and showed that specific features, such as length and nature of backbones and side chains; location, distribution, and density of cationic groups; hydrophilic-hydrophobic balance; and water solubility play critical roles in modulating the electrostatic and hydrophobic interactions between CCOE/CCPE and bacterial outer cell envelope. They have also shown that depending on the backbone length, CCOEs can work either like a membrane stabilizing or altering agent.[47,46,43] Whitten et al.[26,39,34,45,48] treated the bacteria with cationic poly(thiophene), oligo/poly(phenyleneethynylene) under dark and light-activated conditions. They used electron- (TEM), force- (AFM), and fluorescence microscopy to visualize the cell wall's physical structure/morphology, the formation of aggregates,[45] location of disruption/damage on cell envelope,[48] and release of cytoplasmic materials[34] upon treatment. These observations helped them to identify the structural parameters of CCOEs/CCPEs causing bacterial surface alterations. They also predicted that CCPEs usually bind to and form a coating on the outer cell envelope of bacteria; while, the needle-like CCOEs, the small molecular counterparts of CCPEs, intercalate within the lipid bilayers.[26] Many research groups agreed with Whitten's proposed mechanisms (based on morphological observation) that during coating/intercalation, the outer membrane of bacteria, especially the lipid bilayers, experience moderate to significant perturbation[34,42,45,18, 31,49,35] which has a major role in cell lysis and/or growth inhibition of bacteria. [31,49,35,18] Some of the specific lipid bilayer alteration modes

identified or predicted for cationic antimicrobial agents, include, destabilizing of the lipid bilayer (by removal of divalent metal cations),[50,51] lipid bilayer remodeling,[52] bleb/vesicle formation,[48,26,53,54] release of lipid compounds,[55,56] lipid clustering or phase segregation,[55,56] membrane permeabilization,[54,53,50] and so on.

While the morphological feature identification has been used as a tool to propose lipid layer alteration and antimicrobial mechanism, to confirm a specific kind of alteration of the bacterial outer cell envelope, we need extensive experimental approaches which can address the following: (i) unraveling the conjugated polymer-induced compositional alterations of bacterial outer membrane, (ii) composition of extracellular formations (like vesicle/micelle like formations seen in AFM images) or released compounds, (iii) connection of these compositional changes with the changes in quantitative values of mechanical properties of bacterial cell membrane upon treatment. Although, many research works have been done in designing and synthesizing efficient antimicrobial cationic conjugated molecules, very little is done to put such extensive and concerted efforts to deeply understand the antimicrobial action mechanism of CCPE. In some relevant works, total mass of released lipopolysaccharide[46] was measured to understand the role of polymer chain length on membrane stabilization/alteration, or fatty acid analysis[33] was done to explore the increase/decrease in specific kind of fatty acids when bacteria (untreated) was rendered resistance to CCOE on purpose. Performing the lipidomics and fatty acid analysis to understand the lipid/fatty acid loss due to treatment can take our understanding of CCOE/CCPE's antimicrobial mode of action to another level.

In this work, we thus took a holistic approach to explore the morphological, mechanical, and compositional changes of the outer cell envelope of wild-type and amp-resistant *E. coli* upon treatment with a promising phenylene-based, π-conjugated polyelectrolyte P1 (Poly{[2,5-bis(2-(*N,N,N*-triethylammonium)ethoxy)-1,4-phenylene]-alt-1,4-phenylene}, Figure 1) having cationic quaternary amine groups at the side chains. In our previous work,[57] we have shown that a 3-min treatment using P1 retains the viability of the parent bacteria cells, but is able to inhibit the further growth of both wild-type and amp-resistant bacteria very efficiently (~99% growth inhibition). We also put efforts to compare the antimicrobial activities of P1 with that of CCPEs studied so far following such "treat (in PBS buffer)-then grow (in LB media)" method. We found that in order to achieve 70% growth inhibition, we need 15 μM of P1 which was within the range

of concentration of CCPEs (reported by others)[37] needed to achieve similar % growth inhibition. All of these suggested that our P1 can be a potential antimicrobial agent, and deserves more attention towards its action mechanism.

To study morphological changes of P1-treated bacteria, we employed AFM and TEM techniques. AFM can help to detect the signs of cell lysis, cell wall damage, or other morphological alterations (such as the formation of holes, bulges, large blebs, rough surface patches, filamentation, and more) of the outer cell envelope of bacteria cells as a result of treatment with antibacterial agents with nanoscale resolution.[8,45,53,58–60] On the other hand, TEM is beneficial to identify further details of ultrastructural changes (such as small blebs) of the bacterial cell wall.[34,61,62] In addition to AFM and TEM imaging, we performed AFM nanoindentation experiments which gave us the quantitative values of Young's modulus of bacteria cells before and after treatment with P1. Of different techniques to quantify Young's modulus of cells,[63–67,68] AFM nanoindentation stands unique for its capability to visualize the cells and map elastic modulus across the cells simultaneously. The mechanical and morphological properties obtained in this work using these techniques provided complementary information to our prior growth inhibition studies.[57] In order to understand further the cell wall alteration and exposure/loss of lipids, we stained the untreated and P1-treated *E. coli* cells with lipophilic Nile Red dye and imaged them with CLSM. This helped to determine if lipophilic entities of the outer cell envelope were getting surface-exposed due to treatment. Finally, lipidomics and fatty acid analysis were performed to provide concrete evidence of lipid loss and resulting compositional alterations of the bacterial outer cell envelope. We also extended the lipidomics study to unravel the composition of the released components seen as vesicle-like formations around the cells in AFM images. The morphological and compositional information helped us to justify the changes in the elastic modulus of P1-treated cells and explain the bacterial growth inhibition mechanism. Adopting such an all-rounded approach to unveil the action mechanism of CCPEs more precisely can effectively assist and guide the efforts to design new ranges of CCOEs/CCPEs to fight against antibiotic resistance.

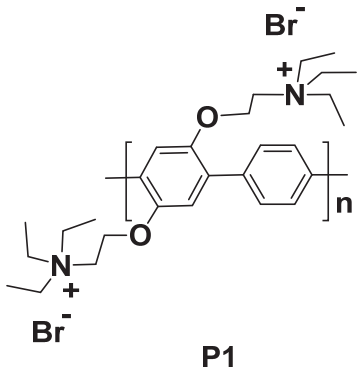

Figure 1. Structure of cationic π-conjugated polyelectrolyte (P1) used in this work.

EXPERIMENTAL SECTION

Cationic π-conjugated polymer synthesis. Neutral π-conjugated polymer, Poly{[2,5-bis(2-(*N*,*N*-diethylamino)ethoxy)-1,4-phenylene]-*alt*-1,4-phenylene} (M_n of 8.8 kg/mol (PPP standard); PDI 2.05) was purchased from Sigma-Aldrich (678066, St. Louis, MO). This neutral π-conjugated polymer was quaternized to yield cationic, π-conjugated polyelectrolyte (P1) following the procedure mentioned in our previous work.[57] All the solvents and reagents needed for the reaction and purification were purchased from commercial suppliers (Sigma-Aldrich (St. Louis, MO), TCI America (Portland, OR), Acros organics (Fair lawn, NJ)). Tetrahydrofuran (THF) (Acros Organics, NJ), used in the quaternization reaction, was distilled from Na/benzophenone under an inert atmosphere. The rest of the reagents and solvents were used without further purification.

Bacterial cultures. Wild-type *E. coli* (DH10B) was obtained from New England Biolab (Ipswich, MA). The ampicillin-resistant (amp-resistant) *E. coli* strain (SSBIO2) was transformed according to our previous work.[57] The strains were stored and cultured following the procedure we reported earlier.[57] Briefly, cells were cultured overnight in solid Luria Bertani (LB) media (Miller, AMRESCO, Solon, OH). A single colony was then transferred into 4 mL of liquid LB media and incubated overnight at 37 °C in a shaker-incubator at 250 rpm. The cells were collected by centrifugation (4700 rpm) for 15 min as pellets. The pellets were washed twice with 5 mM phosphate buffer saline (PBS, Fisher Scientific, Hampton, NH), and resuspended in 5 mM PBS buffer. A Genesys 10S UV-Vis spectrophotometer (Thermo Fisher Scientific, Waltham, MA) was used to measure and adjust the optical density of cells at 600 nm (OD_{600}) further.

AFM sample preparation. Briefly, 900 μL of bacterial suspension (OD_{600} = 0.2) and different concentrations of P1 (0, 30 and 100 μM) were mixed and incubated for 1 h in culture tubes (37 °C, 250 rpm). The treated cells were collected by centrifugation (4700 rpm, 15 min) as pellets. The pellets were washed twice with DI water and resuspended in 1 mL of DI water. Afterward, 50 μL of this suspension was added on top of clean glass slides and allowed to dry overnight at room temperature in a dark place. The air-dried samples were subsequently used for AFM imaging. For Young's modulus measurement, samples that were prepared this way were fixed using glutaraldehyde (Sigma-Aldrich, St. Louis, MO) following the reported protocol[69,70] to ensure that cells did not move during the modulus measurement. At first, the samples were fixed with 0.5 vol% of glutaraldehyde in 5 mM PBS buffer and kept in room temperature for 1 h. This was followed by a second fixing using 1 vol% glutaraldehyde in 5 mM PBS; the samples were then kept at room temperature for 4 h. Fixed cells were washed thrice with DI water, dehydrated sequentially using 20, 30, 50, 70, 90 and 100 vol% of ethanol (Decon Labs, King of Prussia, PA) and used for force measurement.

AFM Imaging. The morphological changes of the *E. coli* cells before and after treatment with P1 were studied using a high-resolution AFM with a built-in inverted optical microscope (MFP-3D-BIO AFM; Oxford Instruments Asylum Research, Santa Barbara, CA). Tapping-mode AFM imaging was carried out on the air-dried samples to study the bacterial surface morphology and measure surface roughness. Once a cluster of bacteria was found with the inverted optical microscope, a 500 × 500 nm^2 and 5 × 5 μm^2 scan with scan rate of 0.2 Hz and 256 scanning lines were carried out. An AC240TS silicon cantilever (Olympus Microcantilevers, Tokyo, Japan) with nominal spring constant of 10.06 N/m and nominal tip radius of 7 nm was used for imaging the samples. In addition, surface roughness was measured in 200 × 200 nm^2 regions over the surface of at least 10 bacteria cells using the onboard Igor Pro 15 software (Waveletrics Inc., Portland, OR). The student's t-test using Microsoft Excel 2016 was used to calculate the statistical difference between each group (i.e. (i) untreated wild-type and treated wild-type *E. coli* cells, (ii) untreated amp-resistant and treated amp-resistant *E. coli* cells, and (iii) untreated wild-type and untreated amp-resistant *E. coli* cells). The ** symbol represents $p < 0.05$ and *** represents $p < 0.0005$ when compared with untreated cells, and the p-value for two datasets < 0.05 was considered to be significantly different (one dataset is significantly different from the other).[53]

AFM force and elastic modulus measurement. AFM nanoindentation was used to get the quantitative value of Young's modulus. Briefly, in this method, the cantilever moves vertically toward the cell until the cantilever tip encounters the cell surface. The cantilever tip is then pressed into the cell surface to perform an indentation, and subsequently raised until the tip is no longer in contact with the cell surface. During this process (which can be repeated many times over an entire cell surface to create a force map), the vertical deflection of cantilever is measured.[71–74] The nominal spring constant (k) for this cantilever is determined using the thermal resonance method. By relating the system parameters (e.g. cantilever spring constant, k) and measured quantities (e.g. cantilever vertical deflection, d) to contact mechanics theory, the applied force (F) is obtained. Simultaneous measurement of the indentation depth (displacement) yields the force-displacement curve (Figure S2), the least-squares fitting of which gives the Young's modulus of the sample.[71–74]

Force mapping was performed in air on the bacteria samples. A TR400PB silicon nitride cantilever (Olympus Microcantilevers, Tokyo, Japan) was used for force mapping. The nominal spring constant (k) for this cantilever was determined as 33.5 ± 0.8 pN/nm. Bacteria clusters consisting of 5-15 bacteria cells within a ~7 × 7 μm^2 area were selected for force mapping. A total of 4096 measurements were performed within this area. Only the measurements in the close vicinity of the apex of bacteria cells were desired in subsequent analysis to avoid artifacts from edge curvature of the cells[75] and non-bacteria indentation tests. Therefore, the unwanted measurements were masked using the Mask function in the Igor Pro 15 software. The force curves were fitted to the Johnson-Kendall-Roberts (JKR)[76] model using Igor Pro 15 to obtain the elastic modulus of bacteria (see Supporting Information for details). Finally, student's t-test was performed (same as AFM imaging section) for comparing the force mapping results for untreated and treated cells. Also, the mean squared errors (MSE) for force curve fits were calculated using a built-in MATLAB code.

Sample Preparation for TEM. The morphological changes of the *E. coli* cells before and after treatment with P1 were studied using bright field high-resolution transmission electron microscopy (HRTEM) (FEI Tecnai Osiris S/TEM) operated at 200 kV. Briefly, 900 μL of bacterial suspension (OD_{600} ~ 0.2) and different concentrations of P1 (0 and 100 μM) were mixed and incubated for 1 h in a shaker-incubator (37 °C, 250 rpm). The treated cells were

separated by centrifugation (4700 rpm, 15 min). The obtained pellets were washed twice with DI water and then centrifuged (4700 rpm, 15 min) again. The obtained cell samples were then fixed in 2.5% glutaraldehyde, and post-fixed with 1% osmium tetroxide. Afterward, the samples were dehydrated sequentially with ethanol (30%, 50%, 75%, 95%, and 100%), followed by acetone. Then, the samples were embedded in resin blocks using the low viscosity embedding media, Spurr's kit (Electron Microscopy Sciences, Hatfield, PA). After that, a Leica EM UC7 ultramicrotome (Leica Camera Company, Wetzlar, Germany) was used to make 100 nm thick cross-sections. Finally, the cross-sections were stained using uranyl acetate and lead citrate, embedded in copper grid (Ted Pella, Inc., Redding, CA) and used for TEM imaging. All of the chemicals used for TEM sample preparation were purchased from Electron Microscopy Science (Hatfield, PA).

Nile Red staining and CLSM imaging. Nile Red (Santa Cruz Biotechnology Inc., Dallas, TX) as a lipophilic stain was used to stain untreated and P1-treated cells according to the literature.[77,78] Briefly, cells (OD_{600} ~ 0.2) were treated with 0-100 μM of P1 in a shaker-incubator (1h, 37 °C, 250 rpm). The cell suspension was centrifuged (4700 rpm, 15 min) and the pellet was resuspended in 1 mL of 5 mM PBS buffer. A stock solution of 25 mM Nile Red in dimethylsulfoxide (DMSO; Alfa Aesar, Haverhill, MA) was prepared first, and 2 μL of this stock dye solution were added to the bacterial suspensions (untreated and P1-treated) to yield the final concentration of Nile Red as 50 μM in the suspension. The cells were incubated in the dye for 3 h, after which the cells were centrifuged, washed twice with 5 mM PBS and resuspended in the same buffer. For CLSM imaging, 10 μL of these cells were added to glass slides (Home Science Tools, Billings, MT) and covered with coverslips. A Nikon A1R-Ti2 confocal laser scanning microscope (Center for Biotechnology, Beadle center, UNL) with a 60x objective lens was used to image the samples. The Nile Red was excited with a 560 nm laser line and emission was collected from 570-620 nm.

Lipid extraction from bacteria cells for lipidomics and fatty acid analysis. Modified Bligh and Dyer method[79] was used to extract the total lipid content of untreated and treated ([P1] =100 μM for 1 h) amp-resistant *E. coli* cells.[55,80] Briefly, P1-treated cells in 5 mM PBS buffer were centrifuged at 4700 rpm for 15 min. After two times washing with DI water, pellets (containing cells) were resuspended in 2 mL DI water. To initiate the extraction, the samples were

transferred to Pyrex glass centrifuge tubes. 5 mL chloroform and 2.5 ml methanol was added to each of these samples (chloroform/methanol (2:1, v/v)). Samples were homogenized with vigorously inverting the tubes and then vortex mixing for 30 seconds. The samples were incubated in ice for 3.5 h, and centrifuged for 10 min at 2000 rpm. The organic lower phase containing lipids were transferred to clean Pyrex glass centrifuge tubes and extraction was repeated two more times. Finally, extracted samples were dried under nitrogen flow, transferred to 2 ml glass vials (~ 2 mg samples/vial), and carried to Kansas Lipidomics Research Center (Manhattan, KS). Xevo TQ-S mass spectroscopy (Waters Co., Milford, MA) and Agilent 6890N GC coupled to an Agilent 5975N quadrupole mass selective detector (Agilent Technologies, Santa Clara, CA) were used to analyze the lipids and fatty acids, respectively. These experiments were performed in 5 replicates, and the lipid or fatty acid contents (nmol) were normalized by the total number of cells. In addition, student's t-test was used to analyze the statistical difference between the treated and untreated samples.

Vesicle separation from cells for SEM, lipidomics and fatty acid analysis. Untreated and P1 treated amp-resistant *E. coli* cells were gently vortexed and filtered three times using 0.2 μm filter papers. Separated vesicles were imaged using SEM (Nova NanoSEM450, FEI, Hillsboro, OR) at Nebraska Center for Materials and Nanoscience. In addition, UV-Vis absorbance of separated vesicles (suspended in DI water) was measured using Perking-Elmer Lambda 40 UV/Vis spectrophotometer (Waltham, MA) to check the presence of the P1 in the extracted vesicles. Finally, samples were freeze-dried and sent for lipidomics and fatty acid analysis.

RESULTS AND DISCUSSION

Morphological alterations of the cell membrane. High-resolution AFM imaging (tapping-mode, in the air) was done to study the morphology of air-dried, untreated, and P1-treated wild-type and amp-resistant *E. coli* cells. Figure 2 shows the AFM height images representing the surface morphology of the cells. The untreated wild-type (Figure 2a) and amp-resistant (Figure 2d) *E. coli* cells were rod-shaped, and the dimensions of the cells (length ~ 1.5-3 μm, height ~ 250 nm) were within the range of values reported for *E. coli*.[81,82] The vague border around the cells could be attributed to slight dehydration of the cells.[82] However, the untreated cells did not

show any sign of lysis[58] which indicated that we were able to consistently follow the AFM sample preparation procedure reported by others.[45,53,82]

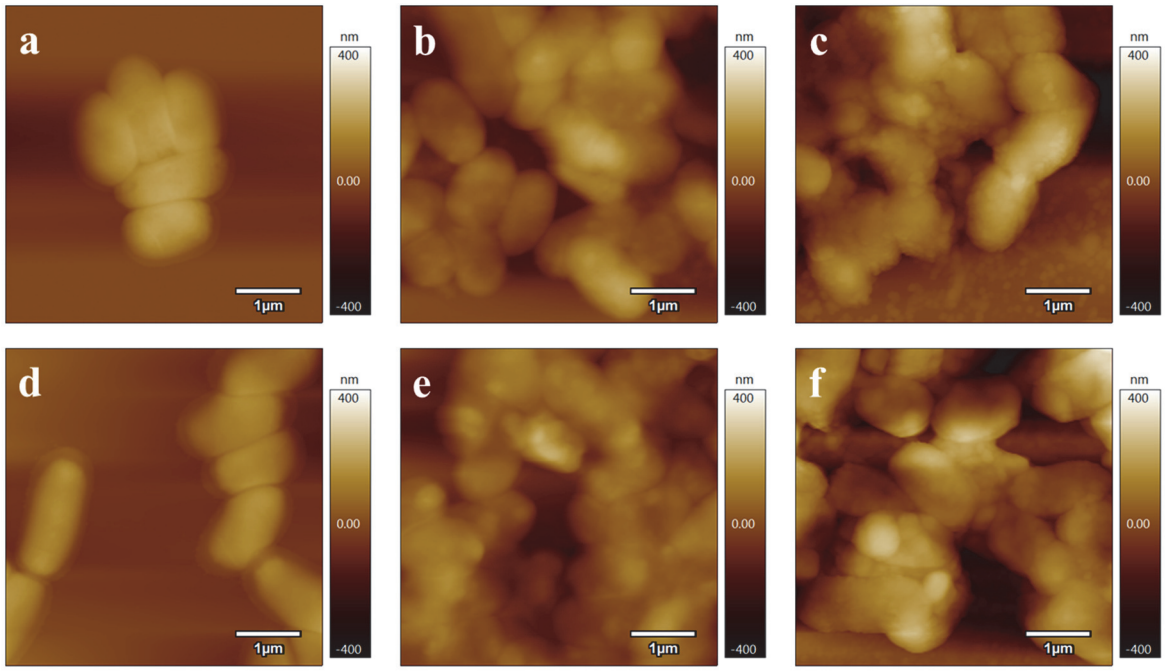

Figure 2. AFM height images of wild-type (a-c) and amp-resistant (d-f) *E. coli* cells treated with 0 (a, d), 30 (b, e), and 100 (c, f) µM P1.

We saw no significant differences in height images between untreated wild-type and amp-resistant *E. coli* cells. However, the same cells showed significant aggregation after treatment with 30-100 µM P1 (Figure 2b, c, e, f). In our previous work, we saw similar growth inhibition trends (up to 99%) and changes in zeta potential (-40 mV (untreated) to +15-20 mV (P1-treated)) when both wild-type and amp-resistant *E. coli* were incubated with P1.[57] This suggested the likelihood of similarity in P1's interaction with both wild-type and amp-resistant strains. Untreated cells typically formed a monolayer (Figure 2a, d), but the aggregation of P1-treated cells (Figure 2b, c, e, f) was observed in directions both parallel and perpendicular to the substrate (as treated cells showed more white-color coded areas (corresponding to height ~ 400 nm), while untreated cells showed heights ~250 nm). We have reported similar observations of three-dimensional aggregation before, based on SEM images of the same cells.[57] The extent of aggregation appeared to increase when the concentration of P1 in the treatment solution was increased from 30 µM (Figure 2b, e) to 100 µM (Figure 2c, f). Since the bacteria surface is net-

negatively charged and P1 is positively charged, the electrostatic interactions (proved by zeta potential changes[57]) between them can coat P1 on the outer cell envelope of the bacteria.[45,57] Moreover, when some bacteria cells are coated with cationic P1, these P1-bacteria complexes can attract some more net negatively charged bacteria towards the P1coating and drive the cell aggregation.

The AFM height images (Figure 2) also allowed us to quantify the average surface roughness of P1-treated and untreated bacteria (Figure 3). To calculate the roughness, a first-order flattening process was applied to the AFM height images.[83,84] Then, 30 (200 × 200 nm^2) regions were randomly selected on at least 10 bacteria cells, and the statistical significance of the differences between the data were obtained using the student's t-test.[53]

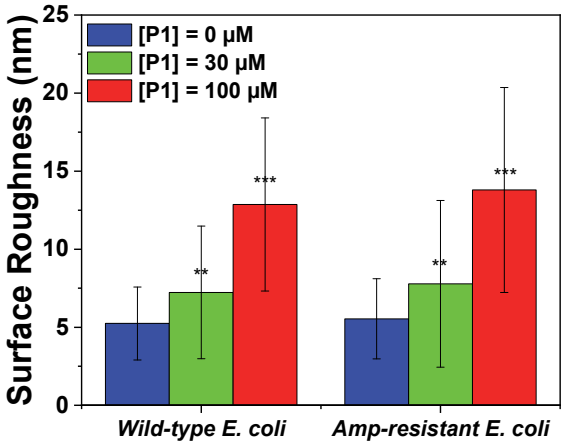

Figure 3. The average surface roughness values (with standard deviation) of untreated wild-type and amp-resistant *E. coli* cells (blue), treated with 30 μM (green), and 100 μM (red) P1. In the AFM height images (after first order flattening process), 30 (200×200 nm^2) regions were randomly selected on at least 10 cells and used for roughness measurement. An unpaired t-test was used for calculating the p-value. The symbol ** represents $p < 0.05$ and *** represents $p < 0.0005$ when compared with untreated cells.

The average surface roughness of untreated wild-type (5.25 ± 2.34 nm) and amp-resistant (5.54 ± 2.56 nm) *E. coli* cells were similar (Figure 3). A gradual increase in surface roughness was observed when the cells were treated with 0 -100 μM P1. When the cells were treated with 100

μM P1, the surface roughness of wild-type and amp-resistant *E. coli* cells increased to 12.88 ± 5.54 nm and 13.79 ± 6.56 nm, respectively (Figure 3). The t-test of these roughness datasets suggested that the treatment with P1 caused a significant change in the roughness of both wild-type and amp-resistant *E. coli*, with a value of $p < 0.0005$. A p-value for two datasets < 0.05 is considered to be statistically significant[33] (i.e. one dataset is significantly different from the other). The t-test values also showed that there was no significant difference between the surface roughness values of the untreated wild-type and untreated amp-resistant *E. coli* cells. Increase in surface roughness due to treatment was also observed for *E. coli* cells treated with phenyleneethynylene-based π-conjugated CCPEs.[45] In some reports, an increase in surface roughness was attributed to the loss of components (such as from O-antigen layer) from LPS,[85] but there may be loss of other components or other mechanisms in action (discussed later).[6,50,53,54,86–88]

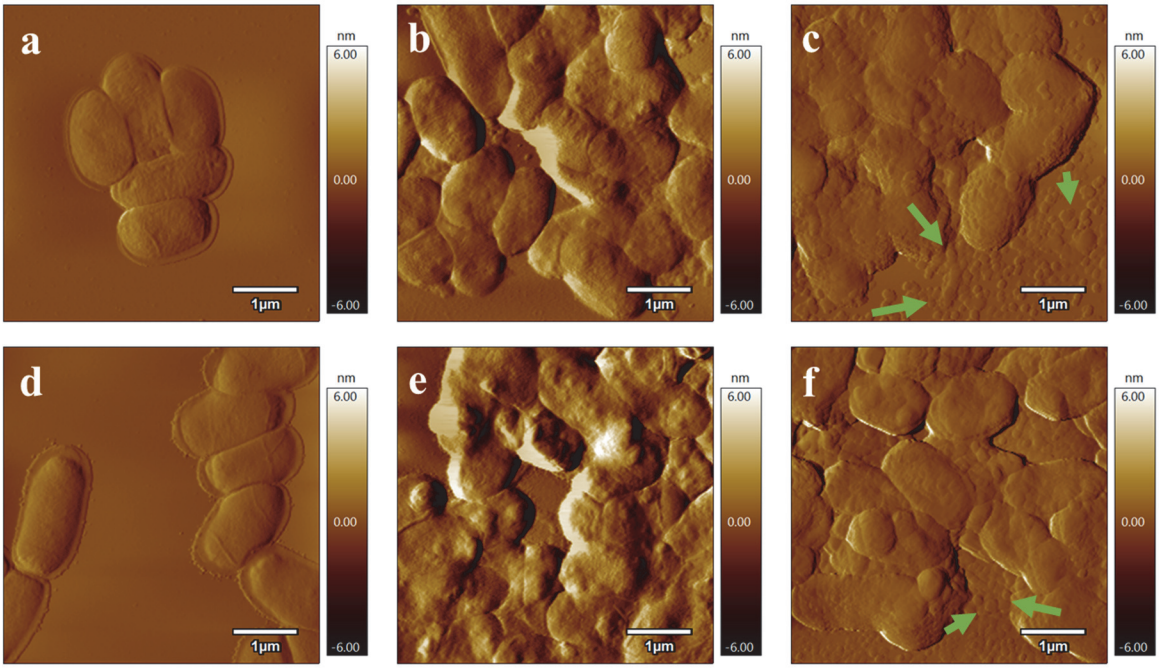

Figure 4. AFM amplitude images of wild-type (a-c) and amp-resistant (d-f) *E. coli* cells treated with 0 (a, d), 30 (b, e), and 100 (c, f) μM P1.

The cell surface roughening observed in AFM height images was consistent with the signs of deformation observed in AFM amplitude images (Figure 4). Vesicular/micellar features ~100 nm in diameter were observed mostly around the treated cells (Figure 4b, c, e, f (shown with the

green arrow)) and some on the surface of the cells (Figure 4b, c, e, f). The formation of vesicles/micelles became most prominent when the cells were treated with 100 μM P1 (Figure 4c, f). Similar observations (formation of vesicle/micelle like structures) have been reported by others for cells treated with cationic antimicrobial agents.[53,54,89,90,91]

In search of how the extracellular vesicle-like structures were formed, we found that ionic drugs such as ethylene diamine tetraacetic acid (EDTA),[92], and gentamicin[93] can sequester/replace the divalent metal cations (Ca^{+2}, Mg^{+2}) from the LPS layer. These metal cations are responsible for stabilizing the lateral repulsion of lipopolysaccharide molecules (net negatively charged) within the LPS layer of healthy cells.[48,92,93] Due to the removal of the metal cations, the LPS layer can destabilize and components from the LPS layer can release to the surroundings of the cells.[48,92,93] In fact, many AMP-based treatment strategies have reported such a simultaneous increase in roughness and release of components from the outer membrane.[6,50,53,54,86–88] Therefore, we hypothesize that the vesicular/micellar formations (Figure 4) and simultaneous surface roughening (Figure 3) are results of detachment/release of lipid-based outer membrane components driven by the electrostatic affinity of cationic P1 towards net-negatively charged lipid moieties. CLSM, lipidomics, and fatty acid analysis were done later to prove this hypothesis and confirm the composition of these released vesicles.

To further investigate the ultrastructural changes of the bacteria cells, TEM images were also captured for untreated and P1-treated amp-resistant *E. coli* with 100 μM P1 (Figure 5). The bacterial outer membranes of untreated amp-resistant *E. coli* cells looked smooth. Also, the contrast (seen in Figure 5a, b) suggested that the intracellular contents of untreated amp-resistant *E. coli* cells were intact. While taking a closer look at the amp-resistant *E. coli* cells treated with 100 μM P1 (Figure 5 c, d), we did not see a drastic increase in contrast at the intracellular region for most of the cells (> 85% cells in a single frame, Figure 5c). This suggested that there was no release of cytoplasmic content[34,45,48,94] upon P1 treatment. In addition, most of the treated cells did not show any other sign of drastic deformation,[34,45,48] extensive tearing,[95] or loss of integrity.[34,45,48,95] This was in agreement with our prior observations based on live/dead assays where the majority of the P1-treated cells were not dead (< 10% dead).[57] However, we observed the formation of spheroidal protrusions typically referred to as "blebs"[96,97] with dimensions ~ 10-20 nm (indicated with red arrows, Figure 5 c, d) from the outer membrane of treated cells.

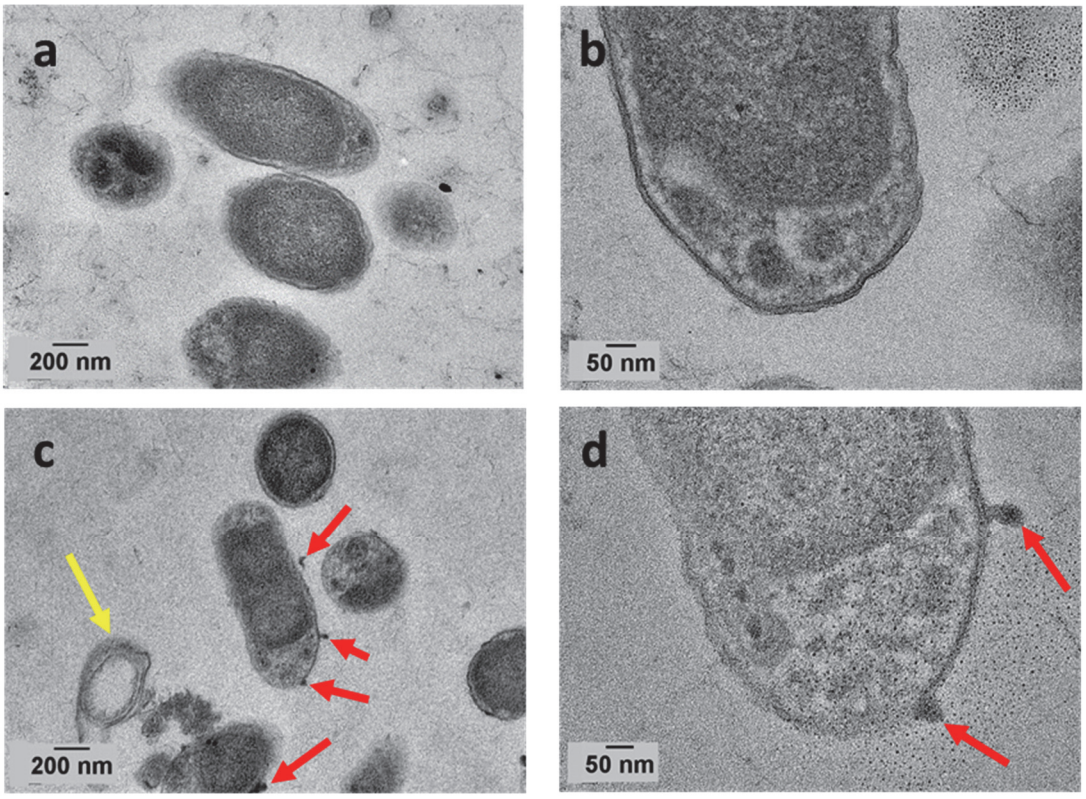

Figure 5. TEM micrographs of untreated (a, b) and 100 μM P1-treated (c, d) amp-resistant *E. coli* cells. The cells were stained with uranyl acetate and lead acetate. The elliptical and circular shapes seen for intact cells were due to the orientation of the cells during the cross-section of the samples using the ultramicrotome. Red arrows indicate the formation of blebs, while the yellow arrow indicates a treated *E. coli* cell from which cytoplasmic content was released.

An obvious question could be why the vesicles seen in AFM images (Figure 4) were not visible in TEM images (Figure 5). This could be due to a very different sample preparation procedure for TEM (as compared to AFM) that required sample fixation and embedding in resin. Similarly, the blebbing seen in TEM images were not visible in AFM images because such nanoscale features (< 10 nm) are hard to resolve with the AFM (radius of the tip ~ 7 nm).[98] However, the blebbing seen in the treated cells was not likely the result of sample preparation steps because the untreated cells looked smooth with a complete absence of blebs in the TEM images (Figure 5a, b).

Bleb formation has been extensively reported for Gram-negative bacteria such as *E. coli*.[61,96,99–101] In many papers, this bleb formation is linked to the interaction[53] or intercalation[62] of cationic antimicrobial compounds with the negatively-charged LPS layer. But, how blebs are formed in response to these interactions still remains elusive, and many mechanisms are proposed.[69,102] Blebbing is associated with (i) the synthesis of defective proteins (upon interaction with antimicrobial compounds) not fitting within the outer membrane;[69] (ii) lipid loss from the outer membrane;[102] and/or (iii) reconfiguration of the outer membrane to accommodate its constituent macromolecules when cationic antibiotics (e.g. aminoglycoside) compete and replace the divalent metal cations[93] to bind with negative charges of lipid-based outer membrane components (e.g. lipid A and phospholipids from lipid bilayer). Especially the remodeling of the outer membrane has been suggested by Whitten and coworkers[34,48] based on the observation of blebs on *E. coli* surfaces upon treatment with phenyleneethynylene-based CCPEs. In a work, it was suggested that the major constituents of outer membrane blebs are outer membrane components.[102] We do not have any experimental evidence at this point of defective protein synthesis. However, the potential of cationic P1 to compete with and replace the divalent metal cations at the net negatively charged junction of lipid A and the inner core of the outer membrane (Figure S1), and the subsequent efforts of the cells to accommodate components of this destabilized LPS layer (i.e. membrane remodeling) seem to rationally explain the bleb formation.

Mechanical alterations of the cell membrane: quantifying elastic modulus. AFM nanoindentation was used to get the quantitative values of Young's modulus by performing force mapping over cells where the cell surfaces were indented using an AFM cantilever.[50,103,104] Typical force-displacement curves from the AFM nanoindentation experiments are shown in Figure S2 for both untreated and P1-treated (with 30 and 100 μM P1) wild-type and amp-resistant *E. coli* cells. The small initial decrease in the force curves from -10 nm until ~ 0 nm of piezo distance, even when the applied force is zero (Figure S2), is an indication of the "jump-to-contact" phenomenon, where the short-range adhesive forces (due to intrinsic tip-sample interactions) caused the tip of the cantilever to jump swiftly to the surface of the cells.[105] Afterwards, as the load on the cantilever increased, the cantilever tip pressed into the outer surface of the bacteria cell. As shown in Figure S2, the slopes of the force curves were lower for P1-treated cells than untreated cells (in both wild-type and amp-resistant *E. coli*). The lower

slope indicated that less force was needed to achieve certain displacement[82] and thus implied that P1-treated cells were less stiff than untreated cells. To quantify the changes in the mechanical properties of the cells before and after treatment, we calculated the Young's modulus of the bacteria using the JKR model to fit the force-displacement data obtained from nanoindentation measurements. While the Hertzian model has been widely used to quantify the elastic modulus of bacteria,[82,103,106] we chose the JKR model for bacteria because this model is best suited for soft samples and accounts for adhesion forces that exist between bacteria and cantilever tip.[105] The fitting of the force curves was performed *via* the Igor Pro 15 software suite (see Supporting Information for details) which gave us the quantitative values of Young's modulus across the bacteria samples. In addition, the mean squared errors (MSE) for force curve fits, calculated for untreated and treated cells, were very small (in the range between 0.01-0.06).

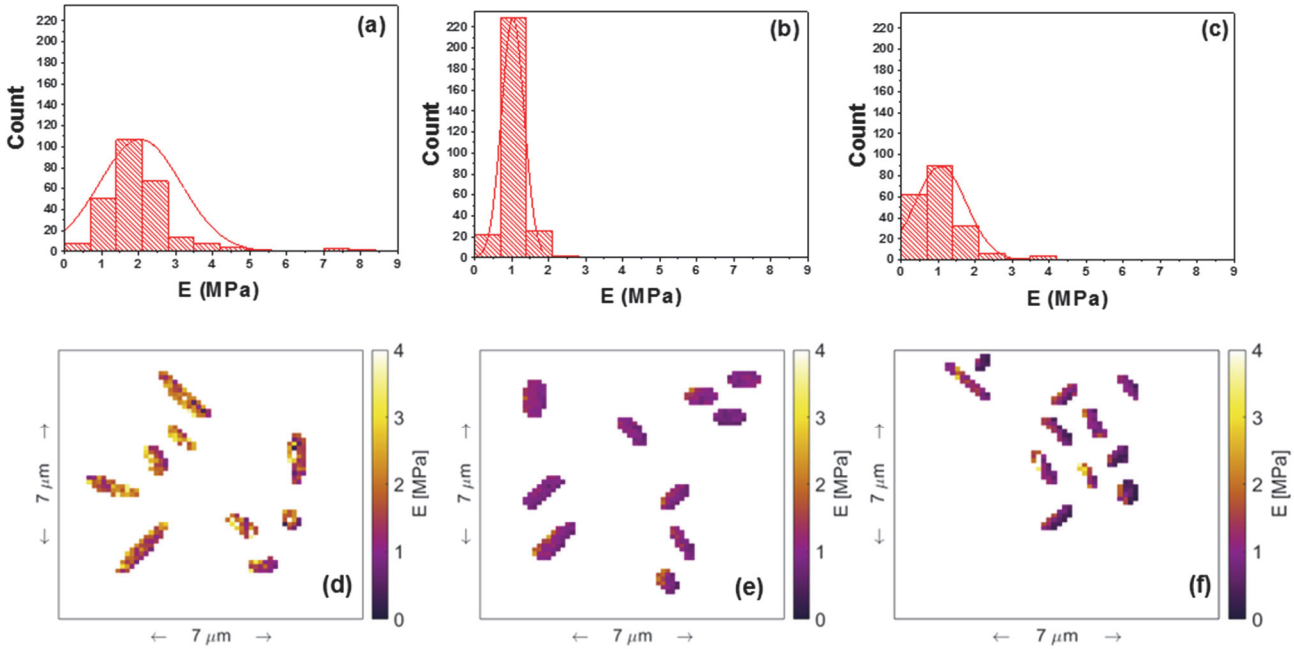

Figure 6. Histograms (with Gaussian distributions (red lines)) of Young's modulus (a-c) and force maps (d-f) for wild-type *E. coli* treated with 0 (a, d), 30 (b, e), and 100 (c, f) μM P1.

The histograms (top panels) and spatially resolved Young's modulus maps (bottom panels) obtained for wild-type and amp-resistant *E. coli* are shown in Figure 6 and Figure 7, respectively. The color-coding of elasticity maps (Figure 6d, e, f, Figure 7d, e, f) indicates how the elastic modulus varies across the *E. coli* cell surfaces. The elasticity maps of untreated wild-type *E. coli* cells were relatively heterogeneous which was reflected by a large Gaussian distribution of

Young's modulus (Figure 6a), with a maximal value of 2.10 MPa and standard deviation of ±1.11 MPa. The Young's modulus of untreated cells closely matched with the reported ones using silicon nitride tips and air-dried cells,[66,107,108] and the standard deviation reported here were also in agreement with literature,[66,106–108,109] where this was attributed to the complexity and heterogeneous distribution of cellular components on cell surfaces. In contrast, the treatment of wild-type *E. coli* cells with 30 μM P1 for 1 h resulted in a more homogeneous elasticity map, consistent with the narrow Gaussian curve for Young's modulus (Figure 6b), with a maximum at ~ 1.03 MPa. The modulus of treated cells (1.03 MPa ± 0.30 MPa) was 50% of that of untreated wild-type cells (2.10 MPa ± 1.11 MPa). This was also evident from the colors in the modulus maps of these samples (Figure 6d, e). The student's t-test confirmed that the Young's modulus data for untreated and 30 μM P1-treated cells were significantly different ($p < 0.05$). These suggested that the surface of P1-treated cells were less stiff than untreated cells. As the P1 concentration was increased from 30 μM (Figure 6b) to 100 μM (Figure 6c), the Young's modulus of wild-type *E. coli* cells (1.07 MPa ± 0.69 MPa) did not change significantly (supported by t-test).

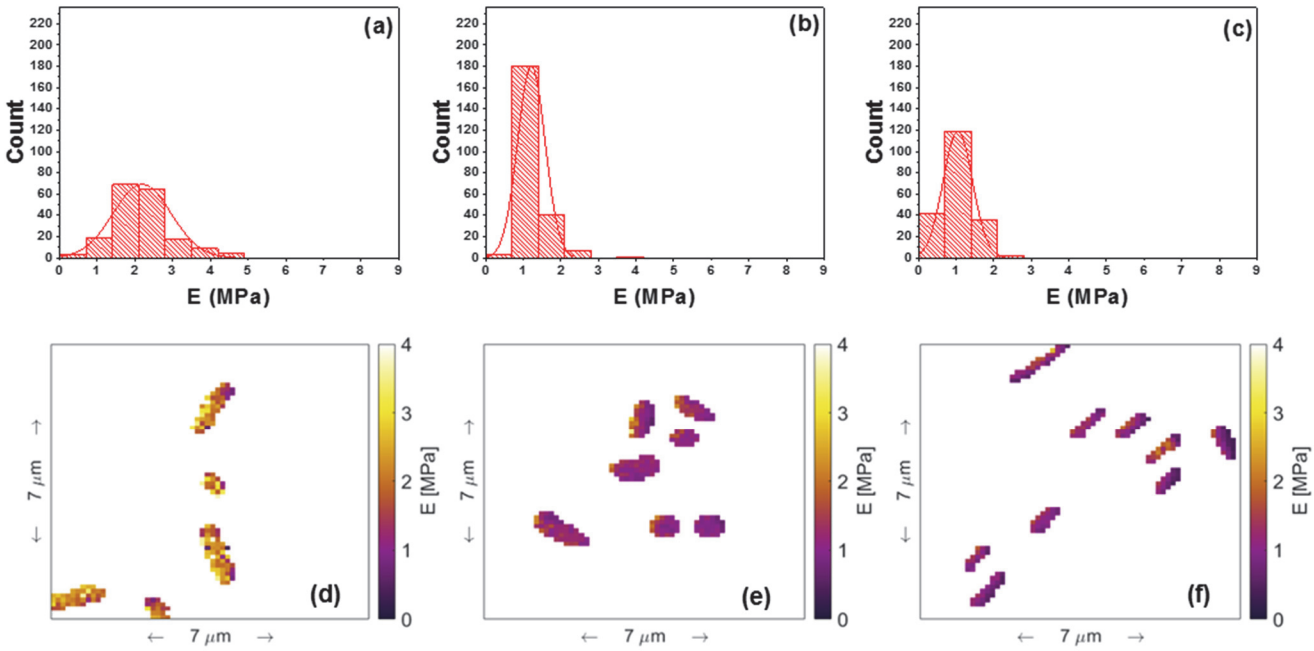

Figure 7. Histograms (with Gaussian distributions (red lines)) of Young's modulus (a-c) and force maps (d-f) for amp-resistant *E. coli* treated with 0 (a, d), 30 (b, e), and 100 (c, f) μM P1.

The Young's modulus of untreated amp-resistant *E. coli* cells (Figure 7a, 2.19 MPa ± 0.77 MPa) was very similar to that of wild-type *E. coli* cells (Figure 6a, 2.10 MPa ± 1.11 MPa) and the difference between them was statistically insignificant ($p > 0.05$). Also, Young's modulus measurement was repeated for untreated wild-type *E. coli* cells. The results (Figure S3) showed that statistically there was no significant difference ($p > 0.05$) between two datasets of wild-type *E. coli* cells (Figure S3) indicating the repeatability of the measurements. In addition, Young's modulus of both 30 and 100 μM P1-treated amp-resistant cells (Figure 7b, c, e, f) decreased in a similar manner as observed for wild-type cells (Figure 6b, c, e, f). This suggested that P1 was likely acting on both wild-type and amp-resistant *E. coli* in a similar manner which was in agreement with similar growth inhibition of these two strains by P1 we reported earlier.[57]

In some of the extreme cases of cell wall damage and release of cytoplasmic content for chitosan,[82] ethylenediamine tetraacetic acid,[110] and streptomycin[110]-treated *E. coli* cells, a decrease in Young's modulus has been reported. We saw a decrease in Young's modulus (Figure 6, 7) in our P1-treated *E. coli* cells which only formed extracellular vesicles and blebs on the cell surface. Such surface alterations appeared to be mild or less damaging (as compared to disruption/ destruction of peptidoglycan layer,[108,111] or release of cytoplasmic content[110]) to be considered as causes of cell lysis/death. Having said that, prior studies suggested that mild alterations, such as the reduction in packing[50]/alignment[112] within the LPS layer, release of lipid-based components,[44,50] and, the formation of blebs[113] can cause a decrease in stiffness of cells (not limited to bacteria cells). While no report on the effect of bleb formation on the stiffness of bacteria cells was found, a study on Xenopus cranial neural crest cells[113] revealed that the blebbing regions of the cells can have lower stiffness than their non-blebbing regions. Vesiculation, on the other hand, is likely the result of LPS destabilization and release of charged lipid components from lipid A and phospholipid bilayers (discussed earlier),[54,89] and such changes can also make the cell wall lose stiffness. Further analysis of lipid loss and composition of released vesicles justified this observed decrease in elastic modulus upon treatment with P1.

Compositional alterations of the cell membrane. We used Nile Red, a lipophilic dye,[114] to stain the untreated and treated *E. coli* cells (Figure 8). Nile Red emits a strong fluorescence in a lipophilic environment, but it does not show fluorescence in a hydrophilic environment.[115,116] Prior attempts to stain bacterial outer membranes with hydrophilic (such as fluorescein

isothiocyanate (FITC)) and lipophilic (Nile Red) dyes showed that the outer and inner cores of the outer membrane of *E. coli* (consisting hydrophilic moieties, such as glucose, galactose, etc.) were moderately impermeable to lipophilic Nile Red.[78] Therefore, Nile Red could not reach to the lipid bilayers underneath the inner core to stain the cells effectively. In a similar attempt, Lazaro et al.[116] were able to stain only 1.1% of healthy *E. coli* cells using Nile Red. In our experiments, the bright-field images showed a good number of untreated bacteria cells dispersed throughout the whole frame showing negligible signs of aggregation (Figure 8a). The corresponding fluorescence image (Figure 8c) showed very few points within the frame which were stained with Nile Red. The comparison between bright-field and fluorescence image thus indicated that most of the healthy cells had unexposed lipid layers which were unreachable by Nile Red dye. On the contrary, the bright-field images of treated *E. coli* cells (Figure 8b) showed aggregation and the corresponding fluorescence image showed that almost all of the cells were stained with Nile Red (Figure 8d), which was an indication of exposure of the lipid regions of the outer membrane upon treatment with P1. These results suggested that the P1 treatment caused a change in the outer membrane of the cells, likely reduced the packing of the outer and inner core and led to a loss of some components of the LPS layer. As a result, the lipid-containing regions (below the inner core) of the outer membrane were largely exposed, making the staining of the treated *E. coli* cells by Nile Red facile. Please note that the vesicles, seen adjacent to cell-P1 complexes in AFM images, could not be resolved in CLSM images due to their small size and Abbe's diffraction limit.[117]

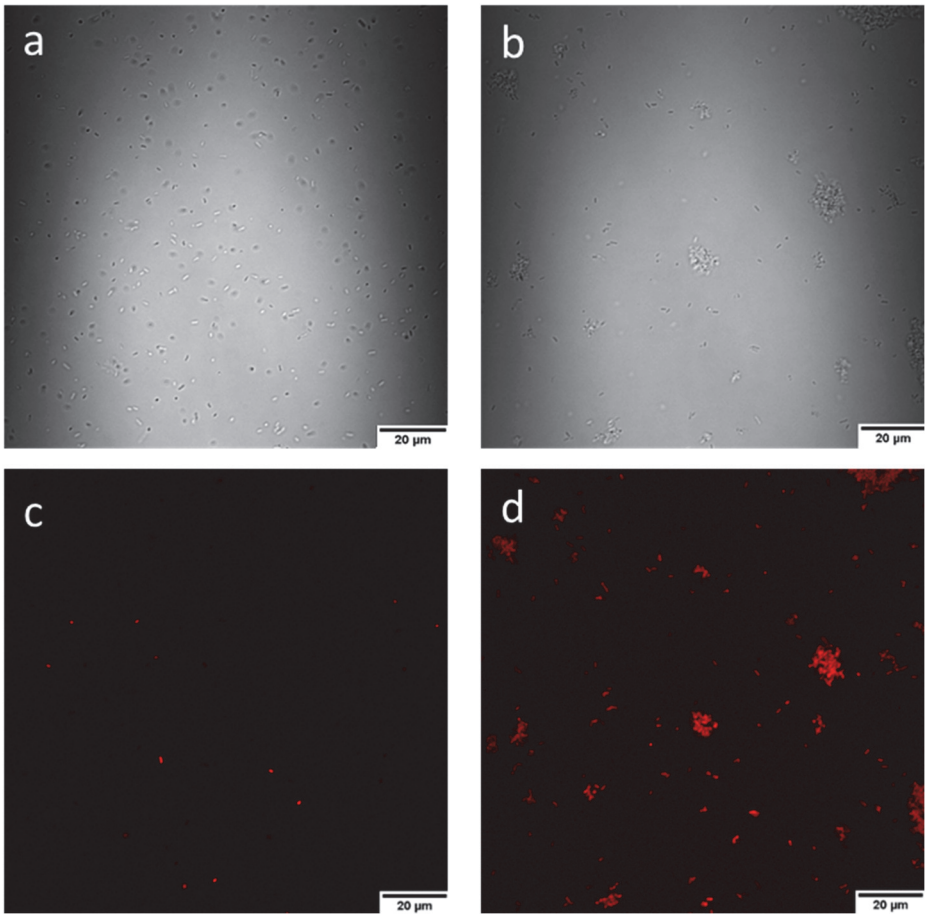

Figure 8. Bright-field (a, b) and fluorescence (c, d) CLSM images of untreated (a, c), and amp-resistant *E. coli* cells treated with 100 µM P1 for 1 h (b, d). The scale bar is 20 µm.

Lipid composition alteration is a common response of cells to stress-induced by antimicrobial agents.[118] Now that we got evidence of loss of components (including lipids) from the outer cell envelope, we wanted to confirm the exact compositional changes due to treatment with P1. In the beginning, we thought that the released components (seen as vesicles in AFM) should be in the supernatant (separated from treated cell suspension). We then took SEM images of supernatant samples separated from both untreated and treated cell suspensions. While the supernatant from untreated cell suspension did not show any vesicle (Figure S4a), the supernatant from treated cell suspension showed only a trace amount of vesicles (Figure S4b). It then appeared more likely that those vesicles, due to electrostatic, hydrophilic, and hydrophobic interactions, adhered/stayed close to the surrounding P1-bacteria complexes and thus did not detach and transfer into the supernatants readily during centrifugation. To work around this, we first

separated the cells from supernatant, resuspended the cells in DI water, and then vortexed the suspension so that the vesicles can detach from the P1-bacteria complexes. Filtering this sample with a 0.2 μm filter allowed the collection of vesicles (please see experimental section for further details). We took SEM image of these collected vesicles where a major fraction of the vesicles had size ~ 100 nm (Figure S5b) (similar to the vesicle dimension seen in AFM images, Figure 4c, f). This further confirmed that using a 0.2 μm filter, we effectively separated the major fraction of released vesicles from the treated cells. A similar effort to collect vesicles from untreated cells and subsequent SEM imaging did not show any vesicle (Figure S5a) which was also in agreement with the complete absence of vesicles seen in AFM image of untreated samples (Figure 4a, d).

In a parallel work, we extracted lipids from amp-resistant *E. coli* cells after treatment with 0 and 100 μM of P1 (please see the experimental section for the details). We then performed lipidomics and fatty acid analysis of the lipids extracted from treated and untreated cells (Figure 9a, b) as well as lipids in released vesicles (Figure S6).

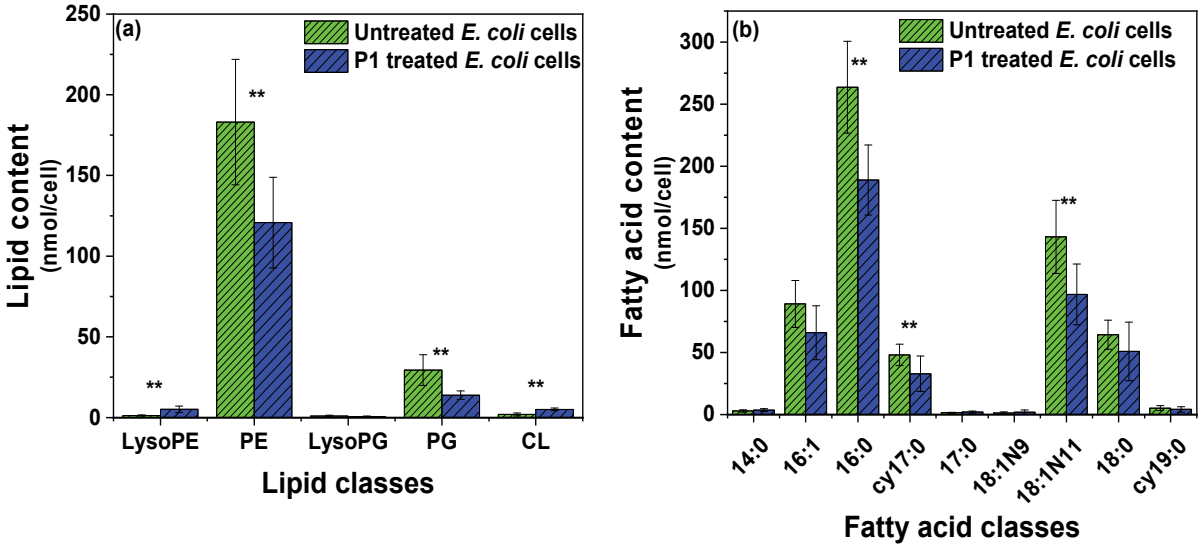

Figure 9. Lipid (a) and fatty acid (b) contents (nmol/cell) in untreated and P1-treated *E. coli* cells. The symbol ** represents $p < 0.05$ and shows a significant difference between the results.

E. coli cells are often reported to have 3 major types of lipids: zwitterionic phosphatidylethanolamine (PE), anionic phosphatidylglycerol (PG), and anionic cardiolipin CL.[119] The % of PE, PG, and CL in a number of *E. coli* strains are reported to be ~75%, 20%, and 5%, respectively.[120,121,119] In addition, the presence of trace amounts of

lysophosphatidylethanolamine (LysoPE) and lysophosphatidylglycerol (LysoPG) are also reported sometimes.[122] It has also been reported that the % of lipids can vary depending on the growth conditions and type of strains of *E. coli* used.[121,123,80,122,55] In our lipidomics experiments, we targeted PE, PG, CL, LysoPE, and LysoPG and found 84.47% PE, 13.58% PG, 0.94% CL, 0.60% LysoPE, 0.40% LysoPG for healthy amp-resistant *E. coli* cells. When we compared the lipid content of untreated and P1-treated cells, we observed a substantial lipid loss upon treatment. A 50% decrease in PG (29.41 ± 9.55 nmol/cell (untreated); 13.84 ± 2.61 nmol/cell (treated)) and 33% decrease in PE (183.07 ± 38.89 nmol/cell (untreated); 120.72 ± 28.12 nmol/cell (treated)) were detected in the treated cells as compared to the untreated ones (Figure 9a). While there was a decrease in both PE and PG content/cell in treated samples, the PE: PG ratio for untreated and treated cells was not statistically significant ($p > 0.05$) suggesting that PE and PG were released from the cells to almost similar extent upon treatment.

In the fatty acid analysis, we found all the major saturated and unsaturated fatty acids present in any *E. coli* sample.[80,124–126,55] The saturated fatty acids we found in our extracted lipid samples from both untreated and treated *E. coli* were: tetradecanoic acid (C14:0), hexadecanoic acid (C16:0), heptadecanoic acid (C17:0), and octadecanoic acid (C18:0). On the other hand, we found the following unsaturated fatty acids: palmitoleic acid (C16:1), two isomers of C18:1 (oleic acid (C18:1N9), vaccenic acid (C18:1N11)), cyclopropyl C17:0 (9,10-methylenehexadecanoic acid (cy17:0)) and cyclopropyl C19:0 (11,12-methyleneoctadecanoic acid (cy19:0)). In agreement with lipidomics results, fatty acid analysis (Figure 9b) also showed a decrease in the fatty acid content of bacteria cells when treated with P1. The major losses we identified were as follows: 29% decrease in C16:0, 33% decrease in C18: 1, 27% decrease in C16:1, 21% decrease in C18:0 and 37% decrease in cy17:0.

Next, we analyzed the vesicles released upon the treatment of amp-resistant *E. coli* cells with P1 and collected via filtration (as discussed earlier). The lipid composition of the released vesicles (from P1-treated cells) was as follows: PE (51%), PG (41%), and the rest were CL, lysoPE, and lysoPG (8%) (Figure S6a). The fatty acid analysis identified the presence of C16:0 (27%), C18:0 (66%), and C18: 1 (7%) in these released vesicles (Figure S6b). While these analyses only confirmed the presence of lipid or fatty acid-based components in the released vesicles, our UV-Vis data showed the characteristic absorbance peaks of P1 (at 285 nm and 330 nm) from the

released vesicle samples (Figure S7). Based on all these concrete evidences, we were able to prove our prior hypothesis (made after AFM image analysis) that the vesicles released from *E. coli* cells after treatment with P1 were composed of charged lipid moieties and cationic P1.

This significant lipid and fatty acid loss explain membrane destabilization, decrease in elastic modulus (Figure 6, 7), and surface-exposed lipid moieties (CLSM, Figure 8) seen for P1-treated *E. coli* cells. The Young's modulus of cells is correlated to membrane composition and cell structure.[13,127] We observed a significant decrease in saturated fatty acids which are known to be responsible for high cell rigidity and low membrane fluidity.[128,129] Bazan et al.[33] showed that an increase in vaccenic acid makes the bacteria more tolerant to CCOE. We saw a 33% decrease in vaccenic acid (C18:1N11) which made the bacteria more vulnerable to attack by P1. Moreover, cyclopropane fatty acids can improve the stability of the membrane under extreme conditions.[33] We observed a loss of a major cyclopropane fatty acid (cyC17:0) which supported the membrane destabilization upon treatment with P1. The observed morphological and mechanical changes can also be explained in light of the observed phospholipid loss as a result of treatment with P1. The degree of order of lipid acyl chains in membranes has been shown to depend on zwitterionic phospholipid components (such as PE here) in anionic model membranes.[130] Thus a loss of PE (33% in our case) can be a good reason for membrane disorder and destabilization thereby. On the other hand, due to the oppositely charged nature, there is an obvious electrostatic interaction between cationic P1 and anionic PG and CL. During such electrostatic interactions, P1 can replace the divalent metal cations (Ca^{+2}, Mg^{+2}) present in the outer membrane. Based on studies on AMPs, replacing these metal cations with cationic antimicrobial agents significantly alters the natural charge distribution within lipid bilayers[51] which is critically needed for membrane stability and integrity. Thus the treatment with cationic P1 can destabilize the outer membrane by increasing intermolecular repulsion between phosphate groups of adjacent lipid moieties in Lipid A and phospholipid regions, loosening/reduction in packing, and simultaneous exposure (increased Nile red staining) and release (lipidomics) of some of the lipid-based charged components from outer membrane giving vesicle/micelle-like structures around treated cells (AFM). The compromised integrity and packing of outer cell envelope clearly explained the decrease in elastic modulus of P1-treated cells. A schematic illustrating these effects is shown in Figure 10.

Sometimes lipid loss and vesiculation are coined as mechanisms of "buying time" [91] meaning the bacteria lose outer membrane components, while they still tend to survive and retain cell function and metabolism (as cytoplasmic content is affected negligibly by treatment). However, lipids and LPS have a role in outer membrane protein biogenesis, cell integrity, and further cell division.[131,132] Especially, in order to maintain cellular structure and structural integrity during cell division, the outer membrane, peptidoglycan layer, and inner membrane have to coordinate and synchronously move towards the middle of the parent cell to create a "pinch-point" or "constricted zone."[133] Thus, any damage of the lipid and LPS layer, as we evidenced in this work, may still allow the parent cells to survive, but impede further cell division. This clearly explains the cell viability after treatment with P1, but subsequent efficient growth inhibition (bacteriostasis), like we observed earlier.[57] Inhibiting the growth of bacteria rather than completely disintegrating and releasing its genetic materials to the surroundings can bring environmental benefits and help limit the spread of antibiotic resistance.[134,135]

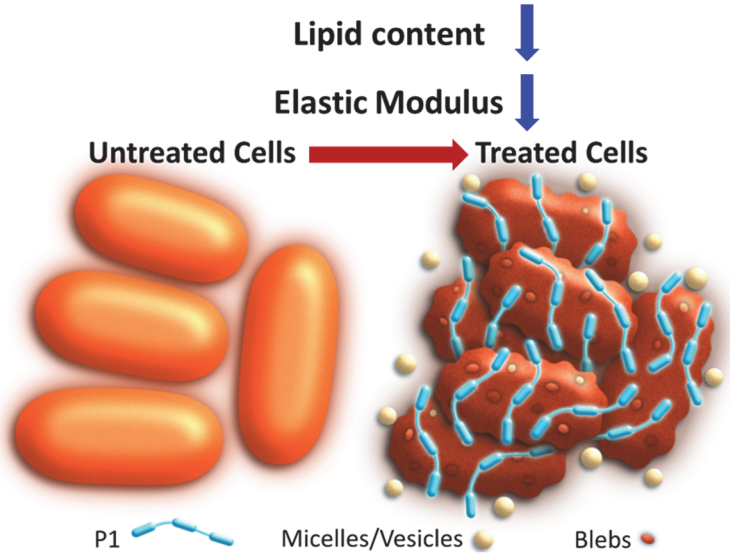

Figure 10. Proposed mechanism of action of P1 on wild-type and amp-resistant *E. coli* cells.

Conclusions. We explored the morphological, mechanical, and compositional changes of the outer cell envelopes of *E. coli* strains upon interactions with a phenylene-based, cationic conjugated polyelectrolyte (P1). As a result of treatment, bacteria surface became rougher (AFM), showed protruded formations, like, blebs at the outer cell envelope (TEM), and formed extracellular vesicles (AFM) around the treated cells. Blebbing could be attributed to the outer

membrane remodeling. An increased staining of P1-treated cells by lipophilic dye Nile Red suggested a loosening of packing of outer cell envelope and release and exposure of lipid-based components. Lipidomics/fatty acid analysis confirmed that the treated cells experienced a noticeable loss in lipids and fatty acids from the outer cell envelope. Moreover, the released vesicles, seen in AFM, were composed of lipid-based charged moieties (PE, PG mainly) and cationic P1 as identified by lipidomics and UV-Vis experiments. Since lipids have a major role in modulating membrane rigidity and integrity, the evidences of lipid bilayer destabilization, disruption, and lipid loss clearly supported the observed decrease in elastic modulus (AFM nanoindentation) of P1-treated cells. Bacteria often alter the outer membrane and/or sacrifice the lipids from the outer membrane as a defense mechanism against losing the cytoplasmic content (based on prior observations of cationic AMPs and antibiotic drugs) as a result of which the parent cells may retain the cell viability. However, the compromised lipid significantly impacts further cell division which rightly explains the efficient growth inhibition (bacteriostatic, rather than bacteriolytic behavior) of both wild-type and amp-resistant bacteria by P1.

ASSOCIATED CONTENT

The supporting information are available at:

AUTHOR INFORMATION

Corresponding Author

sdishari2@unl.edu; Phone: 402-472-7537

Author Contributions

E.Z., T.J.J., R.S., and S.K.D. conceived the idea of the research. E.Z. and T.J.J contributed to this paper equally. S.C. synthesized the conjugated polyelectrolyte. E.Z., C.I., and T.J.J. designed and conducted the experiments exploring the alteration of bacteria surface. A.S. captured the SEM and TEM images. S.K.D. supervised the progress of this whole work and helped E.Z., T.J.J. to analyse the data. Manuscript was written and reviewed by all of the authors.

Notes

The authors declare no conflict of interest.

ACKNOWLEDGMENT

The authors gratefully acknowledge the supports from individual start-up funds from UNL (S.K.D., R.S.) and NSF CAREER Award (NSF-DMR # 1750040) (S.K.D). C.I. acknowledges support from the U.S. Department of Agriculture, National Institute of Food and Agriculture (USDA-NIFA) Postdoctoral Fellowship 2019-67012-29632. The authors thank Nano-Engineering Research Core Facility (NERCF) at UNL for AFM and Nebraska Center for Biotechnology for CLSM measurements. Part of this research (SEM, TEM) was performed in the Nebraska Nanoscale Facility: National Nanotechnology Coordinated Infrastructure and the Nebraska Center for Materials and Nanoscience, which are supported by the National Science Foundation under Award NNCI-1542182, and the Nebraska Research Initiative. The lipid analyses described in this work were performed at the Kansas Lipidomics Research Center Analytical Laboratory. Instrument acquisition and lipidomics method development were supported by the National Science Foundation (including support from the Major Research Instrumentation program; current award DBI-1726527), K-IDeA Networks of Biomedical Research Excellence (INBRE) of National Institute of Health (P20GM103418), USDA National Institute of Food and Agriculture (Hatch/Multi-State project 1013013), and Kansas State University.

REFERENCES

(1) Tacconelli, E.; Carrara, E.; Savoldi, A.; Harbarth, S.; Mendelson, M.; Monnet, D. L.; Pulcini, C.; Kahlmeter, G.; Kluytmans, J.; Carmeli, Y.; Ouellette, M.; Outterson, K.; Patel, J.; Cavaleri, M.; Cox, E. M.; Houchens, C. R.; Grayson, M. L.; Hansen, P.; Singh, N.; Theuretzbacher, U.; Magrini, N. Discovery, Research, and Development of New Antibiotics: The WHO Priority List of Antibiotic-Resistant Bacteria and Tuberculosis. *Lancet. Infect. Dis.* **2018**, *18*, 318–327.

(2) Chang, Y.; Chusri, S.; Sangthong, R.; McNeil, E.; Hu, J.; Du, W.; Li, D.; Fan, X.; Zhou, H.; Chongsuvivatwong, V.; Tang, L. Clinical Pattern of Antibiotic Overuse and Misuse in Primary Healthcare Hospitals in the Outhwest of China. *PloS. one.* **2019**, *14*, 1–12.

(3) Moore, C. E. Changes in Antibiotic Resistance in Animals. *Science.* **2019**, *365*, 1251–1252.

(4) Coates, A. R. M.; Halls, G.; Hu, Y. Novel Classes of Antibiotics or More of the Same? *Br.*

J. Pharmacol. **2011**, *163*, 184–194.

(5) Luepke, K. H.; Suda, K. J.; Boucher, H.; Russo, R. L.; Bonney, M. W.; Hunt, T. D.; Mohr, J. F. Past, Present, and Future of Antibacterial Economics: Increasing Bacterial Resistance, Limited Antibiotic Pipeline, and Societal Implications. *Pharmacotherapy.* **2017**, *37*, 71–84.

(6) Da Silva, A.; Teschke, O. Effects of the Antimicrobial Peptide PGLa on Live Escherichia Coli. *Biochim. Biophys. Acta - Mol. Cell. Res.* **2003**, *1643*, 95–103.

(7) Martinez de Tejada, G.; Sanchez-Gomez, S.; Razquin-Olazaran, I.; Kowalski, I.; Kaconis, Y.; Heinbockel, L.; Andra, J.; Schurholz, T.; Hornef, M.; Dupont, A.; Garidel, P.; Lohner, K.; Gutsmann, T.; A. David, S.; Brandenburg, K. Bacterial Cell Wall Compounds as Promising Targets of Antimicrobial Agents I. Antimicrobial Peptides and Lipopolyamines. *Curr. Drug Targets.* **2012**, *13*, 1121–1130.

(8) Vadillo-Rodriguez, V.; Beveridge, T. J.; Dutcher, J. R. Surface Viscoelasticity of Individual Gram-Negative Bacterial Cells Measured Using Atomic Force Microscopy. *J. Bacteriol.* **2008**, *190*, 4225–4232.

(9) Cui, L.; Ma, X.; Sato, K.; Okuma, K.; Tenover, F. C.; Mamizuka, E. M.; Gemmell, C. G.; Kim, M.; Ploy, M.; Solh, N. El; Ferraz, V.; Hiramitsu, K. Cell Wall Thickening Is a Common Feature of Vancomycin Resistance in Staphylococcus Aureus. *J. Clin. Microbiol.* **2003**, *41*, 5–14.

(10) Pagès, J.; James, C. E.; Winterhalter, M. The Porin and the Permeating Antibiotic: A Selective Diffusion Barrier in Gram-Negative Bacteria. *Nat. Rev. Microbiol.* **2008**, *6*, 893–903.

(11) Jaffe, A.; Chabbert, Y. A.; Semonin, O. Role of Porin Proteins OmpF and OmpC in the Permeation of β-Lactams. *Antimicrob. Agents Chemother.* **1982**, *22*, 942–948.

(12) Fernández, L.; Hancock, R. E. W. Adaptive and Mutational Resistance: Role of Porins and Efflux Pumps in Drug Resistance. *Clin. Microbiol .Rev.* **2012**, *25*, 661–681.

(13) Marín-medina, N.; Ramírez, D. A.; Trier, S.; Leidy, C. Mechanical Properties That Influence Antimicrobial Peptide Activity in Lipid Membranes. *Appl. Microbiol. Biotechnol.* **2016**, *100*, 10251–10263.

(14) Cabeen, M. T.; Jacobs-Wagner, C. Bacterial Cell Shape. *Nat. Rev. Microbiol.* **2005**, *3*, 601–610.

(15) Malanovic, N.; Lohner, K. Gram-Positive Bacterial Cell Envelopes : The Impact on the Activity of Antimicrobial Peptides. *Biochim. Biophys. Acta.* **2016**, *1858*, 936–946.

(16) Chng, S. S.; Ruiz, N.; Chimalakonda, G.; Silhavy, T. J.; Kahne, D. Characterization of the Two-Protein Complex in Escherichia Coli Responsible for Lipopolysaccharide Assembly at the Outer Membrane. *Proc. Natl. Acad. Sci.* **2010**, *107*, 5363–5368.

(17) Martorana, A. M.; Motta, S.; Di Silvestre, D.; Falchi, F.; Dehò, G.; Mauri, P.; Sperandeo, P.; Polissi, A. Dissecting Escherichia Coli Outer Membrane Biogenesis Using Differential Proteomics. *PLoS ONE.* **2014**, *9*, 1–11.

(18) Catania, C.; Thomas, A. W.; Bazan, G. C. Tuning Cell Surface Charge in E. Coli with Conjugated Oligoelectrolytes. *Chem. Sci.* **2016**, *7*, 2023–2029.

(19) Nikaido, H.; Vaara, M. Molecular Basis of Bacterial Outer Membrane Permeability. *Microbiol. Rev.* **1985**, *49*, 1–32.

(20) Kotra, L. P.; Golemi, D.; Amro, N. A.; Liu, G.; Mobashery, S. Dynamics of the Lipopolysaccharide Assembly on the Surface of Escherichia Coli. *J. Am. Chem. Soc.* **1999**, *6*, 8707–8711.

(21) Clifton, L. A.; Skoda, M. W. A.; Daulton, E. L.; Hughes, V.; Brun, A. P. Le; Lakey, J. H.; Holt, S. A.; Clifton, L. A. Asymmetric Phospholipid : Lipopolysaccharide Bilayers ; a Gram-Negative Bacterial Outer Membrane Mimic. *J. R. Soc. Interface.* **2013**, *10*, 1–11.

(22) Silhavy, T.; Kahne, D.; Walker, S. The Bacterial Cell Envelope. *Cold Spring Harb. Perspect. Biol.* **2010**, *2*, 1–16.

(23) May, K. L.; Grabowicz, M. The Bacterial Outer Membrane Is an Evolving Antibiotic Barrier. *Proc. Natl. Acad. Sci. U. S. A.* **2018**, *115*, 8852–8854.

(24) Andersson, D. I.; Hughes, D.; Kubicek-Sutherland, J. Z. Mechanisms and Consequences of Bacterial Resistance to Antimicrobial Peptides. *Drug Resist. Updat.* **2016**, *26*, 43–57.

(25) Moravej, H.; Moravej, Z.; Yazdanparast, M.; Heiat, M.; Mirhosseini, A.; Moghaddam, M. M.; Mirnejad, R. Antimicrobial Peptides: Features, Action, and Their Resistance Mechanisms in Bacteria. *Microb. Drug Resist.* **2018**, *24*, 747–767.

(26) Wang, Y.; Chi, E. Y.; Schanze, K. S.; Whitten, D. G. Membrane Activity of Antimicrobial Phenylene Ethynylene Based Polymers and Oligomers. *Soft Matter* **2012**, *8*, 8547–8558.

(27) Melo, M. N.; Ferre, R.; Castanho, M. A. R. B. Antimicrobial Peptides: Linking Partition, Activity and High Membrane-Bound Concentrations. *Nat. Rev. Microbiol.* **2009**, *7*, 245–

250.

(28) Scheinpflug, K.; Wenzel, M.; Krylova, O.; Bandow, J. E.; Dathe, M.; Strahl, H. Antimicrobial Peptide CWFW Kills by Combining Lipid Phase Separation with Autolysis. *Sci. Rep.* **2017**, *7*, 44332 (1-15).

(29) Omardien, S.; Brul, S.; Zaat, S. A. J. Antimicrobial Activity of Cationic Antimicrobial Peptides against Gram-Positives: Current Progress Made in Understanding the Mode of Action and the Response of Bacteria. *Front. Cell Dev. Biol.* **2016**, *4*, 1–16.

(30) Grage, S. L.; Afonin, S.; Kara, S.; Buth, G.; Ulrich, A. S. Membrane Thinning and Thickening Induced by Membrane-Active Amphipathic Peptides. *Front. Cell Dev. Biol.* **2016**, *4*, 1–13.

(31) Limwongyut, J.; Liu, Y.; Chilambi, G. S.; Seviour, T.; Hinks, J.; Mu, Y.; Bazan, G. C. Interactions of a Paracyclophane-Based Conjugated Oligoelectrolyte with Biological. *RSC Adv.* **2018**, *8*, 39849–39853.

(32) Tian, J.; Zhang, J.; Yang, J.; Du, L.; Geng, H.; Cheng, Y. Conjugated Polymers Act Synergistically with Antibiotics to Combat Bacterial Drug Resistance. *ACS Appl. Mater. Interfaces* **2017**, *9* (22), 18512–18520.

(33) Chilambi, G. S.; Gao, I. H.; Yoon, B. K.; Park, S.; Kawakami, L. M.; Ravikumar, V.; Chan-Park, M. B.; Cho, N. J.; Bazan, G. C.; Kline, K. A.; Rice, S. A.; Hinks, J. Membrane Adaptation Limitations in: Enterococcus Faecalis Underlie Sensitivity and the Inability to Develop Significant Resistance to Conjugated Oligoelectrolytes. *RSC Adv.* **2018**, *8*, 10284–10293.

(34) Wang, Y.; Corbitt, T. S.; Jett, S. D.; Tang, Y.; Schanze, K. S.; Chi, E. Y.; Whitten, D. G. Direct Visualization of Bactericidal Action of Cationic Conjugated Polyelectrolytes and Oligomers. *Langmuir.* **2012**, *28*, 65–70.

(35) Wang, B.; Wang, M.; Mikhailovsky, A.; Wang, S.; Bazan, G. C. A Membrane-Intercalating Conjugated Oligoelectrolyte with High-Efficiency Photodynamic Antimicrobial Activity. *Angew. Chem. Int. Ed.* **2017**, *56*, 5031–5034.

(36) Parthasarathy, A.; Pappas, H. C.; Hill, E. H.; Huang, Y.; Whitten, D. G.; Schanze, K. S. Conjugated Polyelectrolytes with Imidazolium Solubilizing Groups. Properties and Application to Photodynamic Inactivation of Bacteria. *ACS Appl. Mater. Interfaces.* **2015**, *7*, 28027–28034.

(37) Xu, Q.; He, P.; Wang, J.; Chen, H.; Lv, F.; Liu, L.; Wang, S.; Yoon, J. Antimicrobial Activity of a Conjugated Polymer with Cationic Backbone. *Dye. Pigment.* **2019**, *160*, 519–523.

(38) Li, X.; Bai, H.; Yang, Y.; Yoon, J.; Wang, S.; Zhang, X. Supramolecular Antibacterial Materials for Combatting Antibiotic Resistance. *Adv. Mater.* **2019**, *31*, 1805092 (1-28).

(39) Scheberl, A.; Khalil, M. L.; Maghsoodi, F.; Strach, E. W.; Yang, J.; Chi, E. Y.; Schanze, K. S.; Reimhult, E.; Whitten, D. G. Quantitative Determination of Dark and Light-Activated Antimicrobial Activity of Poly(Phenylene Ethynylene), Polythiophene, and Oligo(Phenylene Ethynylene) Electrolytes. *ACS Appl. Mater. Interfaces.* **2020**, *12*, 21322–21329.

(40) Limwongyut, J.; Nie, C.; Moreland, A. S.; Bazan, G. C. Molecular Design of Antimicrobial Conjugated Oligoelectrolytes with Enhanced Selectivity toward Bacterial Cells. *Chem. Sci.* **2020**, *11*, 8138–8144.

(41) He, P.; Lv, F.; Liu, L.; Wang, S. Cationic Conjugated Polymers for Detection and Inactivation of Pathogens. *Sci. China Chem.* **2017**, *60*, 1567–1574.

(42) Zhu, C.; Yang, Q.; Lv, F.; Liu, L.; Wang, S. Conjugated Polymer-Coated Bacteria for Multimodal Intracellular and Extracellular Anticancer Activity. *Adv. Mater.* **2013**, *25*, 1203–1208.

(43) Yan, H.; Rengert, Z. D.; Thomas, A. W.; Rehermann, C.; Hinks, J.; Bazan, G. C. Influence of Molecular Structure on the Antimicrobial Function of Phenylenevinylene Conjugated Oligoelectrolytes. *Chem. Sci.* **2016**, *7*, 5714–5722.

(44) Zhao, Q.; Li, J.; Zhang, X.; Li, Z.; Tang, Y. Cationic Oligo(Thiophene Ethynylene) with Broad-Spectrum and High Antibacterial Efficiency under White Light and Specific Biocidal Activity against S. Aureus in Dark. *ACS Appl. Mater. Interfaces.* **2016**, *8*, 1019–1024.

(45) Edens, L. E.; Wang, Y.; Whitten, D. G.; Keller, D. J. AFM Images of the Dark Biocidal Action of Cationic Conjugated Polyelectrolytes and Oligomers on Escherichia Coli. *Langmuir.* **2014**, *30*, 10691–10697.

(46) Zhou, C.; Chia, G. W. N.; Ho, J. C. S.; Moreland, A. S.; Seviour, T.; Liedberg, B.; Parikh, A. N.; Kjelleberg, S.; Hinks, J.; Bazan, G. C. A Chain-Elongated Oligophenylenevinylene Electrolyte Increases Microbial Membrane Stability. *Adv. Mater.* **2019**, *31*, 1–6.

(47) Hinks, J.; Wang, Y.; Poh, W. H.; Donose, B. C.; Thomas, A. W.; Wuertz, S.; Loo, S. C. J.; Bazan, G. C.; Mu, Y.; Seviour, T. Modeling Cell Membrane Perturbation by Molecules Designed for Transmembrane Electron Transfer. *Langmuir* **2014**, *30*, 2429–2440.

(48) Wang, Y.; Jett, S. D.; Crum, J.; Schanze, K. S.; Chi, E. Y.; Whitten, D. G. Understanding the Dark and Light-Enhanced Bactericidal Action of Cationic Conjugated Polyelectrolytes and Oligomers. *Langmuir.* **2013**, *29*, 781–792.

(49) Catania, C.; Ajo-Franklin, C. M.; Bazan, G. C. Membrane Permeabilization by Conjugated Oligoelectrolytes Accelerates Whole-Cell Catalysis. *RSC Adv.* **2016**, *6*, 100300–100306.

(50) Da Silva, A.; Teschke, O. Dynamics of the Antimicrobial Peptide PGLa Action on Escherichia Coli Monitored by Atomic Force Microscopy. *World J. Microbi. Biot.* **2005**, *21*, 1103–1110.

(51) Lam, N. H.; Ma, Z.; Ha, B. Y. Electrostatic Modification of the Lipopolysaccharide Layer: Competing Effects of Divalent Cations and Polycationic or Polyanionic Molecules. *Soft Matter* **2014**, *10*, 7528–7544.

(52) Shaw, J. E.; Epand, R. F.; Hsu, J. C. Y.; Mo, G. C. H.; Epand, R. M.; Yip, C. M. Cationic Peptide-Induced Remodelling of Model Membranes: Direct Visualization by in Situ Atomic Force Microscopy. *J. Struct. Biol.* **2008**, *162*, 121–138.

(53) Alves, C. S.; Melo, M. N.; Franquelim, H. G.; Ferre, R.; Planas, M.; Feliu, L.; Bardají, E.; Kowalczyk, W.; Andreu, D.; Santos, N. C.; Fernandes, M. X.; Castanho, M. A. R. B. Escherichia Coli Cell Surface Perturbation and Disruption Induced by Antimicrobial Peptides BP100 and PepR. *J. Biol. Chem.* **2010**, *285*, 27536–27544.

(54) Meincken, M.; Holroyd, D. L.; Rautenbach, M. Atomic Force Microscopy Study of the Effect of Antimicrobial Peptides on the Cell Envelope of Escherichia Coli. *Antimicrob. Agents Chemother.* **2005**, *49*, 4085–4092.

(55) Alves, E.; Santos, N.; Melo, T.; Maciel, E.; Dõria, M. L.; Faustino, M. A. F.; Tomé, J. P. C.; Neves, M. G. P. M. S.; Cavaleiro, J. A. S.; Cunha, Â.; Helguero, L. A.; Domingues, P.; Almeida, A.; Domingues, M. R. M. Photodynamic Oxidation of Escherichia Coli Membrane Phospholipids: New Insights Based on Lipidomics. *Rapid Commun. Mass Spectrom.* **2013**, *27*, 2717–2728.

(56) Epand, R. M.; Epand, R. F. Lipid Domains in Bacterial Membranes and the Action of

Antimicrobial Agents. *Biochim. Biophys. Acta - Biomembr.* **2009**, *1788*, 289–294.

(57) Zamani, E.; Chatterjee, S.; Changa, T.; Immethun, C.; Sarella, A.; Saha, R.; Dishari, S. K. Mechanistic Understanding of the Interactions of Cationic Conjugated Oligo- and Polyelectrolytes with Wild-Type and Ampicillin-Resistant Escherichia Coli. *Sci. Rep.* **2019**, *9*, 20411 (1-12).

(58) Braga, P. C.; Ricci, D. Atomic Force Microscopy : Application to Investigation of Escherichia Coli Morphology before and after Exposure to Cefodizime. *Antimicrob. Agents Chemother.* **1998**, *42*, 18–22.

(59) Rossetto, G.; Bergese, P.; Colombi, P.; Depero, L. E.; Giuliani, A.; Nicoletto, S. F.; Pirri, G. Atomic Force Microscopy Evaluation of the Effects of a Novel Antimicrobial Multimeric Peptide on Pseudomonas Aeruginosa. *Nanomed. Nanotech. Biol. Med.* **2007**, *3*, 198–207.

(60) Dufrêne, Y. F.; Boonaert, C. J. P.; Van der Mei, H. C.; Busscher, H. J.; Rouxhet, P. G. Probing Molecular Interactions and Mechanical Properties of Microbial Cell Surfaces by Atomic Force Microscopy. *Ultramicroscopy.* **2001**, *86*, 113–120.

(61) Someya, A.; Tanaka, K.; Tanaka, N. Morphological Changes of Escherichia Coli Induced by Bicyclomycin. *Antimicrob. Agents Chemother.* **1979**, *16*, 87–91.

(62) Chan, E. L.; Harris, R. C.; Dalton, H. P. The Effect of Antibiotics on the Cell Morphology of Legionella Pneumophila. *J. Med. Microbiol.* **1987**, *23*, 149–154.

(63) Schwarz, H.; Koch, A. L. Phase and Electron Microscopic Observations of Osmotically Induced Wrinkling and the Role of Endocytotic Vesicles in the Plasmolysis of the Gram-Negative Cell Wall. *Microbiol.* **1995**, *141*, 3161–3170.

(64) Wood, J. M. Bacterial Responses to Osmotic Challenges. *J. Gen. Physiol.* **2015**, *145*, 381–388.

(65) Amir, A.; Babaeipour, F.; McIntosh, D. B.; Nelson, D. R.; Jun, S. Bending Forces Plastically Deform Growing Bacterial Cell Walls. *Proc. Natl. Acad. Sci. U. S. A.* **2014**, *111*, 5778–5783.

(66) Tuson, H. H.; Auer, G. K.; Renner, L. D.; Hasebe, M.; Salick, M.; Crone, W. C.; Gopinathan, A.; Huang, K. C.; Weibel, D. B. Measuring the Stiffness of Bacterial Cells from Growth Rates in Hydrogels of Tunable Elasticity. *Mol. Microbiol.* **2013**, *84*, 874–891.

(67) Auer, G. K.; Weibel, D. B. Bacterial Cell Mechanics. *Biochem.* **2017**, *56*, 3710–3724.

(68) Schiavone, M.; Formosa-Dague, C.; Elsztein, C.; Teste, M.; Martin-Yken, H.; De Morais, M. A.; Dague, E.; Francois, J. M. Evidence for a Role for the Plasma Membrane in the Nanomechanical Properties of the Cell Wall as Revealed by an Atomic Force Microscopy Study of the Response of Saccharomyces Cerevisiae to Ethanol Stress. *Appl. Env. Microbiol.* **2016**, *82*, 4789–4801.

(69) Rizzello, L.; Sorce, B.; Sabella, S.; Vecchio, G.; Galeone, A.; Brunetti, V.; Cingolani, R.; Pompa, P. P. Impact of Nanoscale Topography on Genomics and Proteomics of Adherent Bacteria. *ACS Nano.* **2011**, *5*, 1865–1876.

(70) Razatos, A.; Ong, Y. L.; Sharma, M. M.; Georgiou, G. Molecular Determinants of Bacterial Adhesion Monitored by Atomic Force Microscopy. *Proc. Natl. Acad. Sci.* **1998**, *95*, 11059–11064.

(71) Lin, D. C.; Dimitriadis, E. K.; Horkay, F. Robust Strategies for Automated AFM Force Curve Analysis - I. Non-Adhesive Indentation of Soft, Inhomogeneous Materials. *J. Biomech. Eng.* **2007**, *129*, 430–440.

(72) Lin, D. C.; Dimitriadis, E. K.; Horkay, F. Robust Strategies for Automated AFM Force Curve Analysis - II: Adhesion-Influenced Indentation of Soft, Elastic Materials. *J. Biomech. Eng.* **2007**, *129*, 904–912.

(73) Bolshakova, A. V; Kiselyova, O. I.; Yaminsky, I. V. Microbial Surfaces Investigated Using Atomic Force Microscopy. *Biotechnol. Prog.* **2004**, *20*, 1615–1622.

(74) Domke, J.; Radmacher, M. Measuring the Elastic Properties of Thin Polymer Films with the Atomic Force Microscope. *Langmuir.* **1998**, *14*, 3320–3325.

(75) Gaboriaud, F.; Parcha, B. S.; Gee, M. L.; Holden, J. A.; Strugnell, R. A. Spatially Resolved Force Spectroscopy of Bacterial Surfaces Using Force-Volume Imaging. *Colloid Surf. B Biointerfaces.* **2008**, *62*, 206–213.

(76) Johnson, K. L.; Kendall, K.; Roberts, A. D. Surface Energy and the Contact of Elastic Solids. *Proc. R. Soc. A.* **1971**, *324*, 301–313.

(77) Pinzon, N. M.; Aukema, K. G.; Gralnick, J. A.; Wackett, L. P. Nile Red Detection of Bacterial Hydrocarbons and Ketones in a High-Throughput Format. *mBio.* **2011**, *2*, 1–5.

(78) Herrera, G.; Martinez, A.; Blanco, M.; O'Connor, J.-E. Assessment of Escherichia Coli B With Enhanced Permeability to Fluorochromes for Flow Cytometric Assays of Bacterial

Cell Function. *Cytometry.* **2002**, *49*, 62–69.

(79) Bligh, E.G. and Dyer, W. J. A Rapid Method of Total Lipid Extraction and Purification. *Can. J. Biochem. Physiol.* **1959**, *37*, 911–919.

(80) Oursel, D.; Loutelier-Bourhis, C.; Orange, N.; Chevalier, S.; Norris, V.; Lange, C. M. Lipid Composition of Membranes of Escherichia Coli by Liquid Chromatography/Tandem Mass Spectrometry Using Negative Electrospray Ionization. *Rapid Commun. Mass Spectrom.* **2007**, *21*, 1721–1728.

(81) Ren, S.; Wu, M.; Guo, J.; Zhang, W.; Liu, X.; Sun, L.; Holyst, R.; Hou, S.; Fang, Y.; Feng, X. Sterilization of Polydimethylsiloxane Surface with Chinese Herb Extract: A New Antibiotic Mechanism of Chlorogenic Acid. *Sci. Rep.* **2015**, *5*, 10464 (1-12).

(82) Eaton, P.; Fernandes, J. C.; Pereira, E.; Pintado, M. E.; Xavier Malcata, F. Atomic Force Microscopy Study of the Antibacterial Effects of Chitosans on Escherichia Coli and Staphylococcus Aureus. *Ultramicroscopy.* **2008**, *108*, 1128–1134.

(83) Liu, B.; Uddin, M. H.; Wah Ng, T.; Paterson, D. L.; Velkov, T.; Li, J.; Fu, J. In Situ Probing the Interior of Single Bacterial Cells at Nanometer Scale. *Nanotechnology.* **2014**, *25*, 415101 (1-13).

(84) Laskowski, D.; Strzelecki, J.; Pawlak, K.; Dahm, H.; Balter, A. Effect of Ampicillin on Adhesive Properties of Bacteria Examined by Atomic Force Microscopy. *Micron* **2018**, *112*, 84–90.

(85) Rittig, M. G.; Kaufmann, A.; Robins, A.; Shaw, B.; Sprenger, H.; Gemsa, D.; Foulongne, V.; Rouot, B.; Dornand, J. Smooth and Rough Lipopolysaccharide Phenotypes of Brucella Induce Different Intracellular Trafficking and Cytokine/Chemokine Release in Human Monocytes. *J. Leukoc. Biol.* **2003**, *74*, 1045–1055.

(86) Ding, L.; Yang, L.; Weiss, T. M.; Waring, A. J.; Lehrer, R. I.; Huang, H. W. Interaction of Antimicrobial Peptides with Lipopolysaccharides. *Biochem.* **2003**, *42*, 12251–12259.

(87) Matsuzaki, K.; Sugishita, K. I.; Miyajima, K. Interactions of an Antimicrobial Peptide, Magainin 2, with Lipopolysaccharide-Containing Liposomes as a Model for Outer Membranes of Gram-Negative Bacteria. *FEBS Lett.* **1999**, *449*, 221–224.

(88) Li, A.; Lee, P. Y.; Ho, B.; Ding, J. L.; Lim, C. T. Atomic Force Microscopy Study of the Antimicrobial Action of Sushi Peptides on Gram Negative Bacteria. *Biochim. Biophys. Acta - Biomembr.* **2007**, *1768*, 411–418.

(89) Dean, S. N.; Leary, D. H.; Sullivan, C. J.; Oh, E.; Walper, S. A. Isolation and Characterization of Lactobacillus-Derived Membrane Vesicles. *Sci. Rep.* **2019**, *9*, 877 (1-11).

(90) Schwechheimer, C.; Kuehn, M. J.; Rodriguez, D. L. Outer-Membrane Vesicles from Gram-Negative Bacteria: Biogenesis and Functions. *Nat Rev Microbiol* **2015**, *13*, 605–619.

(91) Manning, A. J.; Kuehn, M. J. Contribution of Bacterial Outer Membrane Vesicles to Innate Bacterial Defense. *BMC Microbiol.* **2011**, *11*, 1–14.

(92) Amro, N. A.; Kotra, L. P.; Wadu-Mesthrige, K.; Bulychev, A.; Mobashery, S.; Liu, G. Y. High-Resolution Atomic Force Microscopy Studies of the Escherichia Coli Outer Membrane: Structural Basis for Permeability. *Langmuir.* **2000**, *16*, 2789–2796.

(93) Kadurugamuwa, J. L.; Clarke, A. J.; Beveridge, T. J. Surface Action of Gentamicin on Pseudomonas Aeruginosa. *J. Bacteriol.* **1993**, *175*, 5798–5805.

(94) Von Gundlach, A. R.; Garamus, V. M.; Gorniak, T.; Davies, H. A.; Reischl, M.; Mikut, R.; Hilpert, K.; Rosenhahn, A. Small Angle X-Ray Scattering as a High-Throughput Method to Classify Antimicrobial Modes of Action. *Biochim. Biophys. Acta - Biomembr.* **2016**, *1858*, 918–925.

(95) Lenoir, S.; Pagnoulle, C.; Galleni, M.; Compère, P.; Jérôme, R.; Detrembleur, C. Polyolefin Matrixes with Permanent Antibacterial Activity: Preparation, Antibacterial Activity, and Action Mode of the Active Species. *Biomacromolecules.* **2006**, *7*, 2291–2296.

(96) Cushnie, T. P. T.; O'Driscoll, N. H.; Lamb, A. J. Morphological and Ultrastructural Changes in Bacterial Cells as an Indicator of Antibacterial Mechanism of Action. *CELL. MOL. LIFE. SCI.* **2016**, *73*, 4471–4492.

(97) Charras, G.; Paluch, E. Blebs Lead the Way: How to Migrate without Lamellipodia. *Nat. Rev. Mol. Cell Biol.* **2008**, *9*, 730–736.

(98) Tranchida, D.; Piccarolo, S.; Deblieck, R. A. C. Some Experimental Issues of AFM Tip Blind Estimation: The Effect of Noise and Resolution. *Meas. Sci. Technol.* **2006**, *17*, 2630–2636.

(99) Rabanal, F.; Grau-Campistany, A.; Vila-Farrés, X.; Gonzalez-Linares, J.; Borràs, M.; Vila, J.; Manresa, A.; Cajal, Y. A Bioinspired Peptide Scaffold with High Antibiotic

Activity and Low in Vivo Toxicity. *Sci. Rep.* **2015**, *5*, 10558 (1-11).

(100) Koike, M.; Iida, K.; Matsuo, T. Electron Microscopic Studies on Mode of Action of Polymyxin. *J. Bacteriol.* **1969**, *97*, 448–452.

(101) Iida, K.; Koike, M. Cell Wall Alterations of Gram-Negative Bacteria by Aminoglycoside Antibiotics. *Antimicrob. Agents Chemother.* **1974**, *5*, 95–97.

(102) Sutterlin, H. A.; Shi, H.; May, K. L.; Miguel, A.; Khare, S.; Huang, K. C.; Silhavy, T. J. Disruption of Lipid Homeostasis in the Gram-Negative Cell Envelope Activates a Novel Cell Death Pathway. *Proc. Natl. Acad. Sci.* **2016**, *113*, 1565–1574.

(103) Touhami, A.; Nysten, B.; Dufrêne, Y. F. Nanoscale Mapping of the Elasticity of Microbial Cells by Atomic Force Microscopy. *Langmuir.* **2003**, *19*, 4539–4543.

(104) Kuznetsova, T. G.; Starodubtseva, M. N.; Yegorenkov, N. I.; Chizhik, S. A.; Zhdanov, R. I. Atomic Force Microscopy Probing of Cell Elasticity. *Micron.* **2007**, *38*, 824–833.

(105) Efremov, Y. M.; Bagrov, D. V.; Kirpichnikov, M. P.; Shaitan, K. V. Application of the Johnson-Kendall-Roberts Model in AFM-Based Mechanical Measurements on Cells and Gel. *Colloid Surf. B Biointerfaces.* **2015**, *134*, 131–139.

(106) Uzoechi, S. C.; Abu-lail, N. I. Changes in Cellular Elasticities and Conformational Properties of Bacterial Surface Biopolymers of Multidrug-Resistant Escherichia Coli (MDR- E . Coli) Strains in Response to Ampicillin. *Cell Surafce.* **2019**, *5*, 1–15.

(107) Perry, C. C.; Weatherly, M.; Beale, T.; Randriamahefa, A. Atomic Force Microscopy Study of the Antimicrobial Activity of Aqueous Garlic versus Ampicillin against Escherichia Coli and Staphylococcus Aureus. *J. Sci.Food Agric.* **2009**, *89*, 958–964.

(108) Cerf, A.; Cau, J.; Vieu, C.; Dague, E. Nanomechanical Properties of Dead or Alive Single-Patterned Bacteria. *Langmuir.* **2009**, *25*, 5731–5736.

(109) Efremov, Y. M.; Shpichka, A. I.; Kotova, S. A.; Timashev, P. S. Viscoelastic Mapping of Cells Based on Fast Force Volume and PeakForce Tapping. *Soft Matter* **2019**, *15*, 5455–5463.

(110) Li, M.; Gan, C.; Shao, W.; Yu, C.; Wang, X.; Chen, Y. Effects of Membrane Lipid Composition and Antibacterial Drugs on the Rigidity of Escherichia Coli: Different Contributions of Various Bacterial Substructures. *Scanning.* **2016**, *38*, 70–79.

(111) Chinoy, N. J.; Shah, S. D. Mechanisms of Antibiotic Resistance. *HHS Public Access.* **2016**, *4*, 1–37.

(112) Wang, K.; Dang, W.; Yan, J.; Chen, R.; Liu, X.; Yan, W.; Zhang, B.; Xie, J.; Zhang, J.; Wang, R. Membrane Perturbation Action Mode and Structure-Activity Relationships of Protonectin, a Novel Antimicrobial Peptide from the Venom of the Neotropical Social Wasp Agelaia Pallipes Pallipes. *Antimicrob. Agents Chemother.* **2013**, *57*, 4632–4639.

(113) Gonnermann, C.; Huang, C.; Becker, S. F.; Stamov, D. R.; Wedlich, D.; Kashef, J.; Franz, C. M. Quantitating Membrane Bleb Stiffness Using AFM Force Spectroscopy and an Optical Sideview Setup. *Integr. Biol.* **2015**, *7*, 356–363.

(114) Spiekermann, P.; Rehm, B. H. A.; Kalscheuer, R.; Baumeister, D.; Steinbüchel, A. A Sensitive, Viable-Colony Staining Method Using Nile Red for Direct Screening of Bacteria That Accumulate Polyhydroxyalkanoic Acids and Other Lipid Storage Compounds. *Arch. Microbiol.* **1999**, *171*, 73–80.

(115) Greenspan, P.; Mayer, E. P.; Fowler, S. D. Nile Red: A Selective Fluorescent Stain for Intracellular Lipid Droplets. *J. Cell Biol.* **1985**, *100*, 965–973.

(116) Lázaro, B.; Villa, J. A.; Santín, O.; Cabezas, M.; Milagre, C. D. F.; De La Cruz, F.; Moncalián, G. Heterologous Expression of a Thermophilic Diacylglycerol Acyltransferase Triggers Triglyceride Accumulation in Escherichia Coli. *PLoS ONE.* **2017**, *12*, 1–25.

(117) Lipson, S. G.; Lipson, H.; Tannhauser, D. S. *Optical Physics*, 3rd ed.; Cambridge University press: New York, 1995.

(118) Huffer, S.; Clark, M. E.; Ning, J. C.; Blanch, H. W.; Clark, D. S. Role of Alcohols in Growth, Lipid Composition, and Membrane Fluidity of Yeasts, Bacteria, and Archaea. *Appl. Environ. Microbiol.* **2011**, *77*, 6400–6408.

(119) Sohlenkamp, C.; Geiger, O. Bacterial Membrane Lipids: Diversity in Structures and Pathways. *FEMS Microbiol. Rev.* **2015**, *40*, 133–159.

(120) Cronan, J. E. Bacterial Membrane Lipids: Where Do We Stand? *Annu. Rev. Microbiol* **2003**, *57*, 203–224.

(121) Ames, G. F. Lipids of Salmonella Typhimurium and Escherichia Coli: Structure and Metabolism. *J. Bacteriol.* **1968**, *95*, 833–843.

(122) Hines, K. M.; Xu, L. Lipidomic Consequences of Phospholipid Synthesis Defects in Escherichia Coli Revealed by HILIC-Ion Mobility-Mass. *Chem Phys Lipids* **2019**, *219*, 15–22.

(123) Gidden, J.; Denson, J.; Liyanage, R.; Ivey, D. M.; Lay, J. O. Lipid Compositions in

Escherichia Coli and Bacillus Subtilis during Growth as Determined by MALDI-TOF and TOF/TOF Mass Spectrometry. *Int. J. Mass Spectrom.* **2009**, *283*, 178–184.

(124) Oursel, D.; Loutelier-Bourhis, C.; Orange, N.; Chevalier, S.; Norris, V.; Lange, C. M. Identification and Relative Quantification of Fatty Acids in Escherichia Coli Membranes by Gas Chromatography/Mass Spectrometry. *Rapid Commun. Mass Spectrom.* **2007**, *21*, 3229–3233.

(125) Hsu, F.-F.; Turk, J. Characterization of Cardiolipin from Escherichia Coli by Electrospray Ionization with Multiple Stage Quadrupole Ion-Trap Mass Spectrometric Analysis of [M − 2H + Na]− Ions Fong-Fu. *J Am Soc Mass Spectrom.* **2006**, *17*, 420–429.

(126) Kol, M. A.; Kuster, D. W. D.; Boumann, H. A.; De Cock, H.; Heck, A. J. R.; De Kruijff, B.; De Kroon, A. I. P. M. Uptake and Remodeling of Exogenous Phosphatidylethanolamine in E. Coli. *Biochim. Biophys. Acta* **2004**, *1636*, 205–212.

(127) Arnoldi, M.; Fritz, M.; Bäuerlein, E.; Radmacher, M.; Sackmann, E.; Boulbitch, A. Bacterial Turgor Pressure Can Be Measured by Atomic Force Microscopy. *Phys. Rev. E - Stat. Physics, Plasmas, Fluids, Relat. Interdiscip. Top.* **2000**, *62*, 1034–1044.

(128) Zhang, Y. M.; Rock, C. O. Membrane Lipid Homeostasis in Bacteria. *Nat. Rev. Microbiol.* **2008**, *6*, 222–233.

(129) Limonet, M.; Revol-Junelles, A. M.; Milliére, J. B. Variations in the Membrane Fatty Acid Composition of Resistant or Susceptible Leuconostoc or Weissella Strains in the Presence or Absence of Mesenterocin 52A and Mesenterocin 52B Produced by Leuconostoc Mesenteroides Subsp. Mesenteroides FR52. *Appl. Environ. Microbiol.* **2002**, *68*, 2910–2916.

(130) Mason, A. J.; Marquette, A.; Bechinger, B. Zwitterionic Phospholipids and Sterols Modulate Antimicrobial Peptide-Induced Membrane Destabilization. *Biophys. J.* **2007**, *93*, 4289–4299.

(131) Rowlett, V. W.; Mallampalli, V. K. P. S.; Karlstaedt, A.; Dowhan, W.; Taegtmeyer, H.; Margolin, W.; Vitrac, H. The Impact of Membrane Phospholipid Alterations in Escherichia Coli on Cellular Function. *J. Bacteriol.* **2017**, *199*, 1–22.

(132) Bos, M. P.; Robert, V.; Tommassen, J. Biogenesis of the Gram-Negative Bacterial Outer Membrane. *Annu. Rev. Microbiol.* **2007**, *61*, 191–214.

(133) Gray, A. N.; Egan, A. J. F.; Veer, I. L. Van; Verheul, J.; Colavin, A.; Koumoutsi, A.;

Biboy, J.; Altelaar, A. F. M.; Damen, M. J.; Huang, K. C.; Simorre, J.; Breukink, E.; Blaauwen, T. Den; Typas, A.; Gross, C. A.; Vollmer, W. Coordination of Peptidoglycan Synthesis and Outer Membrane Constriction during Escherichia Coli Cell Division. *eLife.* **2015**, *4*, 1–29.

(134) Zhang, X.; Zhang, T.; Fang, H. H. P. Antibiotic Resistance Genes in Water Environment. *Appl. Microbiol. Biotechnol.* **2009**, *82*, 397–414.

(135) Khan, F. A.; Söderquist, B.; Jass, J. Prevalence and Diversity of Antibiotic Resistance Genes in Swedish Aquatic Environments Impacted by Household and Hospital Wastewater. *Front. Microbiol.* **2019**, *10*, 1–12.

TOC Figure